Persistent legacy effects on soil metagenomes facilitate plant adaptive responses to drought

Nichole A. Ginnan[1,2*], Valéria Custódio[3*], David Gopaulchan[3*], Natalie Ford[1,4], Isai Salas-González[5], Dylan D. Jones[3], Darren M. Wells[3], Ângela Moreno[6], Gabriel Castrillo[3#], Maggie R. Wagner[1,4#]

[1] Kansas Biological Survey and Center for Ecological Research, University of Kansas, Lawrence, KS, USA 66045

[2] One Health Microbiome Center, Huck Institutes of the Life Sciences, Penn State University, State College, PA, USA

[3] School of Biosciences, University of Nottingham, Sutton Bonington, UK

[4] Department of Ecology and Evolutionary Biology, University of Kansas, Lawrence, KS, USA 66045

[5] Center for Genomics Sciences. Universidad Nacional Autónoma de México

[6] Ministério da Agricultura e Ambiente, Cabo Verde

[*] These authors contributed equally

[#] Corresponding authors

SUMMARY

Both chronic and acute drought alter the composition and physiology of soil microbiomes, with implications for globally important processes including carbon cycling and plant productivity. When water is scarce, selection favors microbes with thicker peptidoglycan cell walls, sporulation ability, and constitutive osmolyte production (Schimel, Balser, and Wallenstein 2007)—but also the ability to degrade complex plant-derived polysaccharides, suggesting that the success of plants and microbes during drought are inextricably linked. However, communities vary enormously in their drought responses and subsequent interactions with plants. Hypothesized causes of this variation in drought resilience include soil texture, soil chemistry, and historical precipitation patterns that shaped the starting communities and their constituent species (Evans, Allison, and Hawkes 2022). Currently, the physiological and molecular mechanisms of microbial drought responses and microbe-dependent plant drought responses in diverse natural soils are largely unknown (de Vries et al. 2023). Here, we identify numerous microbial taxa, genes, and functions that characterize soil microbiomes with legacies of chronic water limitation. Soil microbiota from historically dry climates buffered plants from the negative effects of subsequent acute drought, but only for a wild grass species native to the same region, and not for domesticated maize. In particular, microbiota with a legacy of chronic water limitation altered the expression of a small subset of host genes in crown roots, which mediated the effect of acute drought on transpiration and intrinsic water use efficiency. Our results reveal how long-term exposure to water stress alters soil microbial communities at the metagenomic level, and demonstrate the resulting "legacy effects" on neighboring plants in unprecedented molecular and physiological detail.

MAIN

Rapid global changes, such as escalating temperatures and changing precipitation patterns, intensify pressure on both natural ecosystems and agricultural systems. Among these changes, the increasing frequency and intensity of droughts are emerging as one of the most formidable challenges, with devastating consequences for plant health and survival. However, soil microbial communities, with their remarkable ability to quickly adapt to environmental shifts (Chase, Weihe, and Martiny 2021), may play a crucial role in bolstering the resilience of plants and ecosystems to drought stress. Additionally, previous exposure to stress can shape the future trajectories of microbial communities and influence their responses to subsequent environmental disturbances, a phenomenon referred to as legacy effects or ecological memory (Canarini et al. 2021). Despite the growing recognition of microbial legacy effects, the mechanisms driving microbiome legacy effects, their long-term persistence, and whether these effects extend uniformly across different plant genotypes remains unanswered. Furthermore, soil properties, such as porosity of

mineral nutrient content can also govern soil microbiomes (Custódio et al. 2022), making it difficult to isolate the effects of precipitation on the microbiome and soil memory development.

Here, to investigate microbial drought legacy effects and isolate the drivers and impacts of microbiome adaptations to water limitation, we evaluate natural microbiome variations across two independent precipitation gradients, test the ability of legacy effects to persist through experimental perturbation, and rigorously evaluate the impacts of microbiome precipitation history on plant responses to acute drought at the molecular and physiological levels. Finally, we assess the extent to which microbiome legacy effects are transferable across plant species. Our results demonstrate that legacy effects of historical exposure to dry conditions are particularly salient at the metatranscriptomic level and trigger transcriptional changes in plant roots that improve resistance to subsequent acute droughts, at least in some plant species.

Soil microbiome composition, mineral nutrient content, and porosity vary across a natural precipitation gradient

To explore the relationship between free-living soil microbiota and water availability in natural environments, we must also understand other soil properties that could impact microbiome local adaptations. First, we identified six never-irrigated, native prairie sites along a steep precipitation gradient in Kansas, USA (Figure 1a and 1b). Shot-gun metagenomic sequencing of soils from these six sites indicated that although bacterial alpha diversity (Shannon diversity) is similar across the natural precipitation gradient (Figure 1c), the bacterial taxonomic composition significantly differed. Between-sample variation showed a strong biogeographic signature (PERMANOVA, $R^2 = 0.11$, $p = 0.001$) and site precipitation explaining 5.3% of the variation (Figure 1d). We compared the relative abundance of bacterial phyla across the soils, and identified an enrichment of Actinomycetota and Bacillota in historically dry soils, while Proteobacteria and Acidobacteriota were enriched in historically wet soils (Extended Data Figure 1a), which is in line with previous findings (Naylor et al. 2017).

To disentangle the influence of soil edaphic properties and precipitation history on the microbiota compositional changes detected across the soils, we first examined the mineral nutrient and trace element profiles of all soils using ICP-MS. Similar to the microbial taxonomic composition, we observed significant mineral nutrient differences, with soil site explaining 27.9% of the variation and precipitation explaining 28.6% (Figure 1e). The soil mineral nutrient profiles separated into two groups along the first principle coordinate axis: the three low-precipitation sites TRI, SVR, and HAY, and the three higher-precipitation sites KNZ, CWR, and WEL. Several individual mineral nutrient concentrations were correlated with the

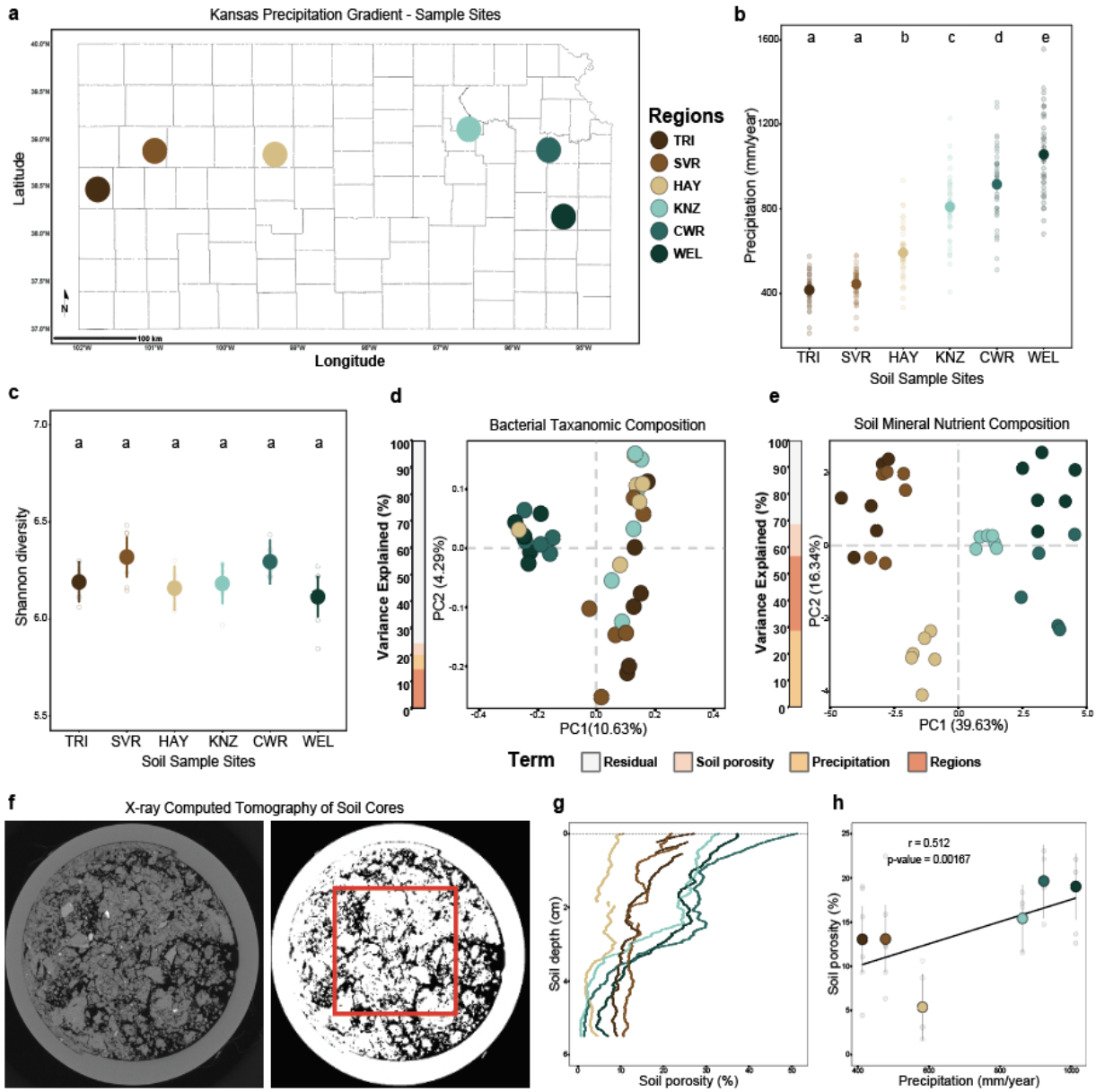

Figure 1. Kansas precipitation gradient soil properties. a) Map of Kansas native prairie soil sample sites along. b) Mean annual precipitation at our six native prairie soil sample sites. c) Bacterial microbial community alpha diversity across soil sites. d) Beta diversity of soil bacterial communities and PERMANOVA results indicating the amount of variation explained by each tested variable. e) Beta diversity of soil mineral nutrients of soil sample sites and PERMANOVA results. f) example of a vertical slice image of an X-ray computed tomography of soil cores used to calculate soil porosity. g) Soil porosity of Kansas soil cores. h) Soil porosity correlates with site precipitation history.

mean annual precipitation (Extended Data Figure 1b,c). Furthermore, we detected a significant correlation (r = 0.384; *p*-value = 1e-04) between the mineral nutrient dissimilarities and the microbiota composition dissimilarities among the soil samples (Extended Data Figure 1d). This suggests that mineral nutrients must be considered when trying to isolate the effects of precipitation.

Next, we used x-ray computed tomography to quantify soil porosity of undisturbed soil cores sampled across the same six sites (Figure 1f). Soil porosity, a measure of the percent of space or pores among soil aggregates, is directly related to soil hydraulic properties (Dexter 2004; Beven and Germann, n.d.). In general, lower porosity results in lower water retention and infiltration. Therefore, it is a good indicator to assess the effect of precipitation on the actual water content in the soil. We found in all cases a decrease in soil porosity with depth and greater porosity in soils exposed to higher precipitation (Figure 1g). Furthermore, we observed a significant positive correlation between the soil porosity and the precipitation gradient across the soil sample sites (Figure 1h). These results suggest that precipitation history might affect soil porosity in surface layers of soils (Rousseva, Torri, and Pagliai 2002), which could affect soil niche properties and, consequently, the abundance of specific microbiota members. Nevertheless, we found no correlation between the soil porosity dissimilarities and the bacterial microbiota composition dissimilarities in these soils (Extended Data Figure 1e), suggesting that soil porosity is not a key element controlling the overall microbiota composition in these soils.

Soil bacterial functional enrichments suggest local adaptations to water availability.

Next, we explored the impacts of precipitation, soil porosity, and soil mineral nutrients on soil bacterial functional potential using the assembled metagenomic contigs. To focus on robust functions that are generally associated with water availability rather than site-specific variation, we collapsed our six soils into two major groups representing our sites with low precipitation (TRI, SVR, HAY) and high precipitation history (KNZ, CWR, WEL). These groupings also preserved the similarities in microbiome taxonomic composition, mineral nutrient content, and porosity revealed by our previous analyses (Figure 1b,d,e,h). We identified 62 Gene Ontology (GO) categories that were differentially abundant in soils exposed to low precipitation *versus* high precipitation (Figure 2a). We identified enrichments in biological processes typically associated with bacterial tolerance to abiotic stress, such as nitrogen cycle metabolic process, fatty acid (a major cell membrane structural component) biosynthetic process, and glucan metabolic process, and DNA repair in our low-precipitation soils (Figure 2a) (Sun et al. 2012; Woodcock et al. 2021; Gil-Quintana et al. 2013) (Figure 2a). These results, therefore, confirm that the natural bacterial communities from our low-precipitation soils are functionally different from our high-precipitation microbiota, and even with multiple soil factors interacting with these communities there is still clear evidence of adaptations to osmotic-stress. Overall, we can conclude that bacterial communities across our natural precipitation gradient are functionally adapted to local precipitation-levels, making them an excellent candidate for exploring potential precipitation legacy effects.

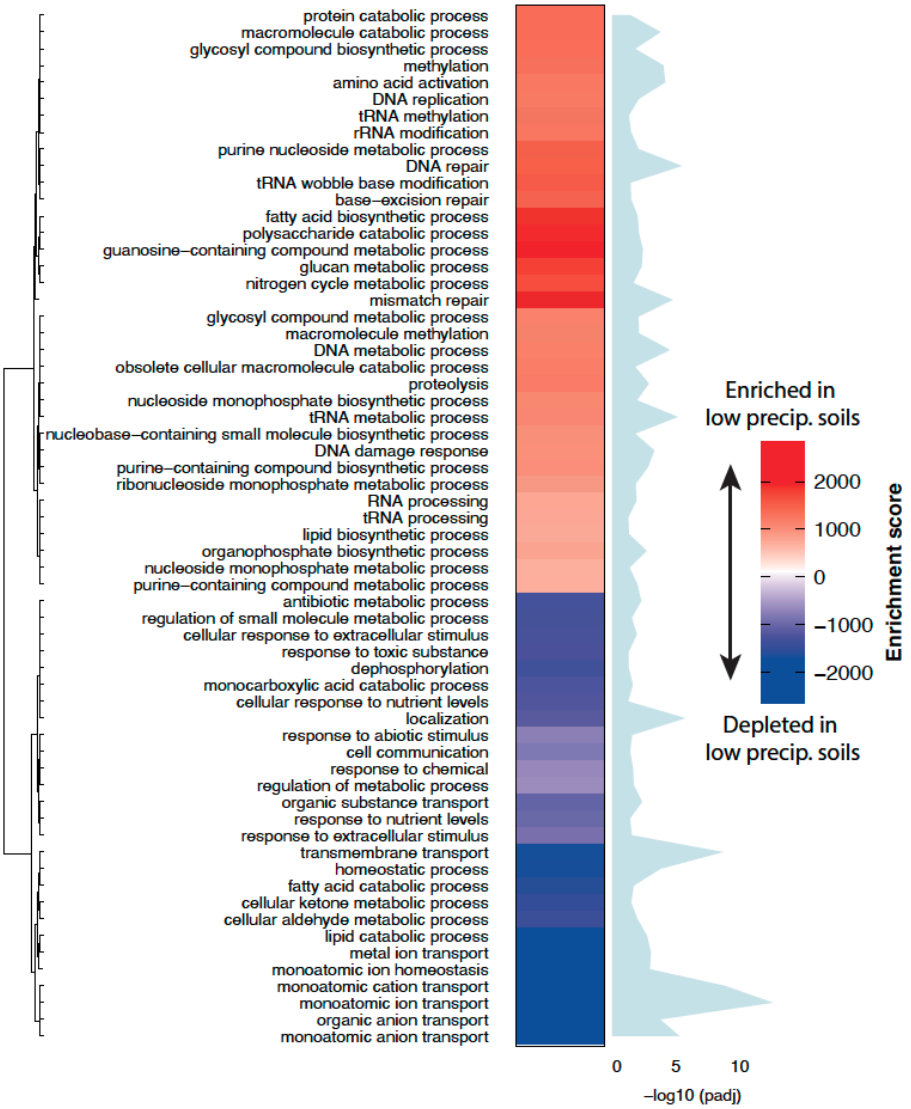

Figure 2. Precipitation history-dependent functional enrichments. Heatmap of Gene Ontology (GO) categories enriched (red) and depleted (blue) in low precipitation history soil microbiomes, as compared to those from high precipitation history soils

Distant natural precipitation gradients have conserved metagenomic properties

To validate that these patterns are generally associated with precipitation patterns, rather than specific to Kansas, we sampled a second, distant, natural precipitation gradient: Santiago island, Cabo Verde. Here, we sampled nine never-irrigated (rain-fed) agricultural sites (Extended data Figure 2a). Compared to the steep Kansas macro-gradient, the Cabo Verde sample sites represent a stable micro-gradient of precipitation (Extended Data Figure 2b). Like in Kansas, bacterial alpha diversity was similar across all soil samples (Extended Data Figure 2c), and the bacterial phylum Actinomycetota was enriched,

while Proteobacteria was depleted in soils with the lowest precipitation (Extended Data Figure 2d). We observed small, but significant differences in bacterial beta diversity among the soils (Extended Data Figure 2e). However, a principal coordinates analysis showed a reduced biogeographic signature in bacterial community composition in Cabo Verde soils compared to Kansas soils (Figure 1d and Extended Data Figure 2e). Cabo Verde has a dry micro-gradient of precipitation, and the sample sites are closer together, which likely explains this observation.

Unlike in the Kansas soils, we did not find a clear separation in the mineral nutrient profiles of the soils that correlated with mean annual precipitation (Extended Data Figure 2f,g), even though several individual mineral nutrients were significantly negatively (Na, Se, Sr) and positively (Cd, B, Mn, Co, Zn, P, Rb, Fe) correlated with precipitation (Extended Data Figure 2h). Furthermore, we confirmed a significant correlation between mineral nutrient dissimilarities and microbiota dissimilarities in these soils ($r = 0.541$; p-value = 1e-04; Extended Data Figure 2i). Therefore, we generalize that the mechanisms controlling mineral nutrient content in soils could also regulate the general characteristics of the composition of free-living bacterial communities in soils exposed to different precipitation rates. Additionally, there were no significant differences in soil porosity (Extended Data Figure 2a), and no correlation between soil porosity and mean annual precipitation, between mineral nutrient content and precipitation, or between soil porosity dissimilarity and microbiota taxonomic dissimilarity in Cabo Verde soils (Extended Data Figure 2d). However, we still identified significant differences in bacterial community functional potential across the soils (Extended Data Figure 3). Indeed, when comparing the abundances of bacterial GO terms between the highest precipitation soil and all of the other Cabo Verde soils, similar categories as those identified in Kansas were enriched and depleted (Extended Data Figure 3 and Figure 2). For example, nitrogen cycle metabolic processes, including ornithine metabolic process and purine nucleoside triphosphate metabolic process, were also found enriched in these soils. Because abiotic stress tends to impair nitrogen fixation and other metabolic processes, this suggests that communities from low-precipitation sites may be adapted to have a greater capacity to fix nitrogen. As in the Kansas soils, several GO categories including ionic homeostasis were depleted in Cabo Verde soils exposed to low precipitation, which could be important for maintaining cell turgor. This indicates that the ecological strategies used by free-living bacteria to cope with water limitation are robust to variation in other edaphic properties and are conserved across multiple, distant, soil sites. From this, we conclude that the functional differences among our Kansas soils accurately represent the legacy effects of chronic water limitation and are likely generalizable to other water-limited soil microbiomes.

Functional legacy effects are resilient to short term perturbations

To assess the effects of short-term perturbations on soil microbiome legacy effects, we exposed the six soils from Kansas to a five-month-long conditioning phase in a growth chamber, during which replicate pots of each soil were either left unplanted or planted with a seedling of the native grass species *Tripsacum dactyloides* (eastern gamagrass), and were either drought-challenged or well-watered, in a factorial design. To confirm that the intensity of our experimental acute drought had physiological consequences in our system, we quantified plant morphological features and anatomical parameters in gamagrass using laser ablation tomography. Shoot height was reduced and the number of aerenchyma in the roots was higher in plants exposed to the acute drought treatment relative to the well-watered plants, demonstrating that the experimental drought was sufficient to impact the plants and, presumably, the soil-dwelling microbes (Extended Data Figure 4a,b). We observed that the *T. dactyloides* plants that received inoculum with a low-precipitation history had increased shoot height, root and shoot mass, and total aerenchyma area under

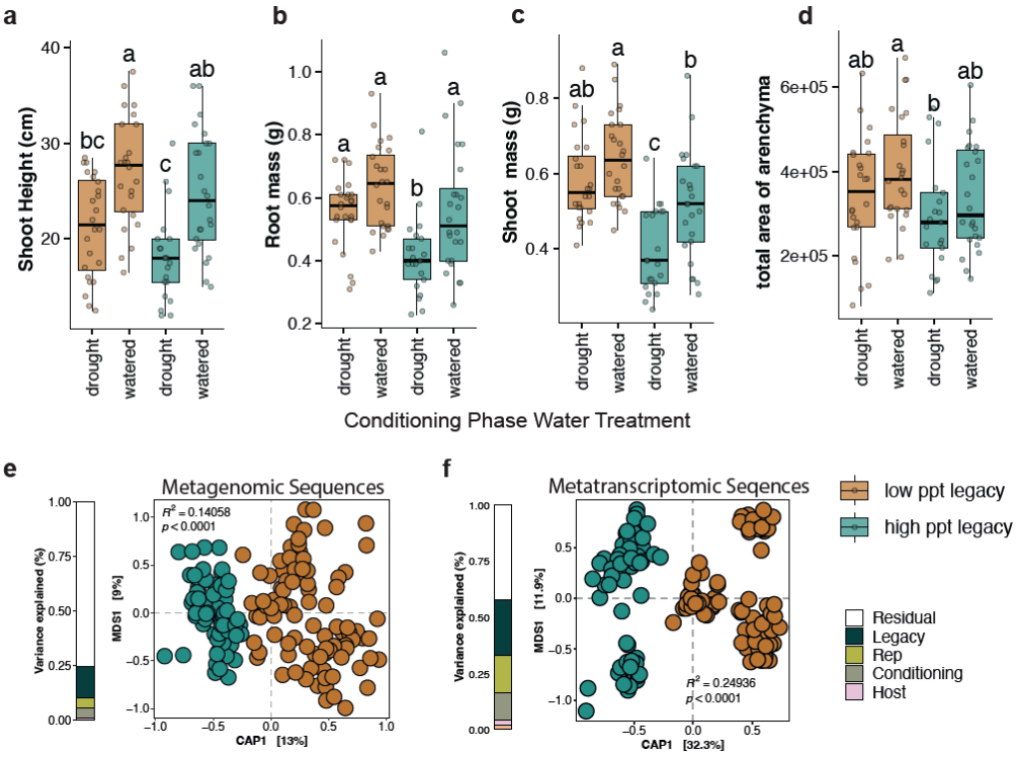

Figure 3. Molecular signatures of precipitation legacy are robust to short-term perturbations. (a-d) *Tripsacum dactyloides* plants grown in mesocosms of dry-legacy soils outperformed those grown in wet-legacy soils during a 5-month-long experimental drought. **(e-f)** By the end of the 5-month-long experimental drought, the dry-legacy and wet-legacy soil microbiomes were clearly distinguishable regardless of whether they were in the droughted or control group, and whether they were grown with or without a host plant. The effects of precipitation legacy were especially prevalent at the metatranscriptomic level (f), indicating that taxonomic similarities among these soil communities belie differences in transcriptional activity.

drought treatment compared to plants that received high precipitation legacy inoculum (Figure 3a,b,c,e), confirming that soil microbiomes' precipitation legacies affect plant phenotypes.

Next, we explored how drought legacy affected the drought response trajectories of free-living (bulk soil) and gamagrass-associated microbial communities (rhizosphere) when exposed to intermittent drought and watering events. Similar to our natural soil community, bacterial community alpha diversity was similar across all treatment groups (Extended Data Figure 4c). There were also no major taxonomic profile shifts across treatments at the phylum-level (Extended Data Figure 4d). However, canonical analysis of principal coordinates of metagenomic sequences indicated that metagenome content was significantly impacted by the conditioning water and host treatments, but only explained 4.3% and 1.1% of the variation in the data, respectively (Extended Data Figure 4e,f). In contrast, precipitation history explained 14.1% of the variation in bacterial community composition (Figure 3e). Interestingly, constrained ordination of metatranscriptome data found that precipitation history explained 24.9% of the variation in microbial gene expression (Figure 3c), while condition water treatment and host treatment explained only 12.3% and 1.8% of the variation (Extended data Figure 5a,b). This demonstrates that the strongest effects of precipitation legacy are on patterns of microbial gene expression, and that both metagenome and metatranscriptome content manifest precipitation legacy more clearly than the taxonomic composition of soil communities. Additionally, the taxonomic, metagenomic, and metatranscriptomic signatures of precipitation legacy are all robust to short-term perturbation.

Subsequently, we examined bacterial biological processes differences driving the changes in beta diversity shown above. We analyzed enrichment in GO terms between low precipitation soils exposed to the different conditioning treatments and the soils with a history of high precipitation. Again, we found a consistent enrichment of GO terms across the low precipitation soils such as nitrogen cycle metabolic process, including purine−containing compound metabolic process, and pyrimidine−containing compound metabolic process, and a depletion of ion transport and amino acid catabolic process that were robust to the perturbations applied. Some of these GO categories were also detected in the free-living communities studied in Kansas and Santiago soils (Figure 2, and Extended Data Figure 3). This indicates that bacterial functional memory is robust to the perturbations applied during the conditioning phase. Our metatranscriptomic data confirmed that genes associated with the differential GO categories were active across treatment groups, and identified significantly different GO categories enriched in drought legacy soils compared to wet legacy soils, such as tetrapyrrole metabolic process, response to osmotic stress, liposaccharide metabolic process, heme metabolic process, and trehalose catabolic process after applied conditioning treatments. Despite perturbations applied for five months, we detected a robust enrichment in the functionally active Actinomycetota and Bacillota phyla in all historically dry soils and an enrichment

in the transcriptionally active Acidobacteriota, Planctomycetota, and Pseudomonadota in all historically wet soils (Extended Data Figure 5c), in line with the findings from our metagenomic sequencing of natural soils in Kansas and Cabo Verde (Extended Data Figure 1a and 2d). Therefore, we confirmed that the long-term precipitation history is functionally robust to short-term (five months) acute conditioning perturbations.

Microbiota precipitation legacy alters host plant responses to subsequent acute drought despite taxonomic convergence of root microbiomes

To assess the functional effects of microbiome precipitation legacy, we used the experimentally-conditioned microbial communities to inoculate a new generation of *T. dactyloides* cv. "Pete" (N=286). These "Test Phase" plants were divided between water-limited conditions (⅔ of all plants) and well-watered control conditions (⅓ of plants). We confirmed that our experimental drought treatment impaired plant growth (Extended Data Figure 6a). We uprooted five-week-old gamagrass plants for phenotyping, 16S rRNA gene microbiome profiling of crown roots, and crown root gene expression analysis. Our focus on bacteria was motivated by past work showing that root-colonizing fungi from these soils were insensitive to drought (Swift et al. 2024) and by our observation that more than 97.3% of all metagenomic reads in this study were bacterial. Our focus on crown roots was motivated by evidence that this root type is highly active in water acquisition (Ahmed et al. 2018), but see (Gao and Lynch 2016). To capture the effects of the precipitation gradient extremes, plant gene expression was measured only for plants that received inocula derived from the two easternmost (wet-legacy) and two westernmost (dry-legacy) soils.

Surprisingly, precipitation legacy did not have a significant effect on either the evenness (Shannon diversity) or the taxonomic composition of the gamagrass root bacterial community as measured by 16S rRNA gene sequencing (Extended Data Figure 6b). The taxonomic composition of the crown root bacterial community was only impacted by the test phase water treatment (Extended Data Figure 6c; ANOVA.CCA, $F_{1,139}$=2.57, R^2=0.016, p=0.004), which only explained 1.6% of the variation in the data. We further assessed root microbiome community stability by calculating beta-dispersion, a measure of within-group variability. Neither test phase water treatment, inoculum legacy, nor their interaction impacted gamagrass root bacterial community beta-diserperion (Extended Data Figure 6d; ANOVA $F_{1,144}$=0.571, p=0.45). Altogether, these results suggest that eastern gamagrass exerts a strong homogenizing influence during root microbiome formation and that its endosphere community is remarkably stable and resistant to water stress. The stability of the gamagrass root bacterial microbiome, even after receiving compositionally different inocula (Figure 3e,f), indicates a deterministic process (not stochastic) of community assembly. Considering the long evolutionary history of eastern gamagrass with prairie soil microbes, the microbiome is likely adapted to this host, which promotes stable community assembly; for instance, previous microbiome passage

experiments in tomatoes showed an increase in microbiome stability and adaptation to host genotype over time (Morella et al. 2020). Furthermore, bacterial experimental evolution with legumes indicates that microbes are more cooperative with a host with which they share a history (Batstone et al. 2020).

Although precipitation legacy did not significantly shape 16S-v4 rRNA gene diversity within the *T. dactyloides* root microbiome, its clear effect on metagenomic diversity and microbial gene expression (Figure 3e,f,g and Extended Data Figure 5c) demonstrated its potential to influence plant phenotype. Indeed, RNA-seq analysis of test-phase plants confirmed that microbial inocula with contrasting precipitation legacies differentially influenced gene expression in the crown roots. In addition to 15 genes that were differentially expressed depending on whether the inoculum originated from a high-precipitation or low-precipitation region (Figure 4a; Supplementary Data 1), we observed that microbial legacy influenced the responses of 183 genes to acute drought stress (Figure 4b). The majority of these were unresponsive to acute drought in plants grown with a dry-legacy microbiota, but were significantly down-regulated or up-regulated in plants grown with a wet-legacy microbiota (Figure 4b, gene sets I and II, respectively), suggesting that the ecological memory of drought transmitted through the soil subdued the overall transcriptional response of gamagrass to acute drought, perhaps allowing the host to conserve energy. The 50 *T. dactyloides* genes that decreased expression under acute drought only in the presence of a wet-legacy microbiome (Figure 4b gene set I) included several that are orthologous to maize genes predicted to be involved in ethylene- or ABA-mediated signaling of water stress (Td00002ba004498, Td00002ba024351, Td00002ba011993, Td00002ba005402, Td00002ba000033) and a heat shock protein linked to temperature stress (Td00002ba042486) (Supplementary Data 1). Notably, the latter three genes were not identified as drought-sensitive when averaging across inocula, demonstrating that the microbial context is necessary for a complete understanding of molecular plant drought responses.

Next, we extensively phenotyped the test phase plants to determine whether microbial precipitation legacy altered host phenotypic responses to a subsequent acute drought. For each of 63 traits, including mineral and nutrient content, mass and height, photosynthesis and gas exchange rates, crown root anatomy, and root system architecture, we calculated a drought susceptibility index (S-index) that measures the stability of a trait under drought relative to control plants that received the same inoculum type ($S=Trait_{drought}/mean(Trait_{control})$). Thus, an S-index of 1 indicates that the trait value of a droughted plant was equal to the mean trait value of the corresponding well-watered control plants. We used a random forest model to rank and identify the ten most important traits for describing the phenotypic effects of microbiome precipitation legacy (Extended Data Figure 7a,b). We then summarized

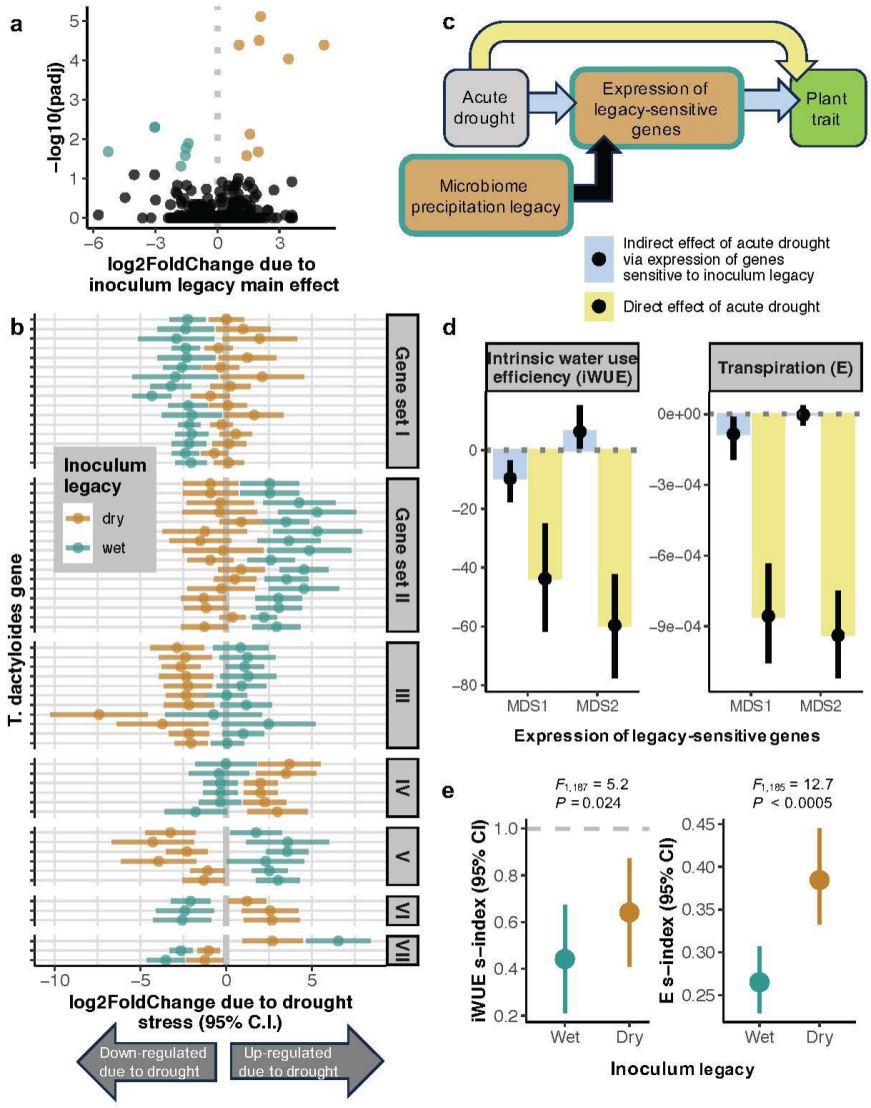

Figure 4. Drought legacy of microbial inocula alters the response to drought in eastern gamagrass. (a) 15 genes were up-regulated in plants inoculated with microbiota from a low-precipitation region, relative to plants inoculated with microbiota from a high-precipitation region. (b) In total, 183 *T. dactyloides* genes responded to acute drought in a manner that was dependent on the drought legacy of the soil microbiota, regardless of the inoculum's treatment during the conditioning phase (Supplementary Data 1). Only genes with a drought response of ≥4-fold and with annotated maize ortholog(s) are shown here for illustration purposes. Each pair of points shows one gene; the relative position of the two points illustrates how the gene's expression changed in response to acute drought during the Test Phase, depending on whether the plant had been inoculated with microbiota derived from a low-precipitation or high-precipitation environment. Genes are grouped into sets according to the pattern of how inoculum legacy altered their drought responses. (c) The model used for mediation analysis to test whether the expression of the 198 legacy-sensitive genes (see panels a-b) contributed to the overall effect of acute drought on plant phenotype. (d) Mediation analysis confirmed that the expression of legacy-sensitive genes is part of the plant response to acute drought resulting in decreased intrinsic water-use efficiency (iWUE) and transpiration (E). (e) Microbiomes with a low precipitation legacy caused increased iWUE and E during acute drought, relative to inocula derived from high precipitation- legacy soils. The s-index describes trait values scaled by the mean value of well-watered control plants, such that an s-index of 1 indicates that droughted plants were phenotypically identical to non-droughted plants.

the variation in these top traits using constrained redundancy analysis, which revealed that microbiome precipitation legacy explained 5% of the total variation in host phenotypic response to acute drought (ANOVA.CCA, $F_{1,187}$=10.1, R^2=0.05, p=0.001) (Extended Data Figure 8a). At the individual trait-level, microbiota precipitation legacy significantly impacted six of the top eight non-correlated traits: transpiration, leaf chlorophyll content, max root width, root total metaxylem area, median root diameter, Cu, K, and intrinsic water use efficiency (iWUE) – an important plant drought response trait (Hund, Ruta, and Liedgens 2009; Schulz et al. 2021)(Extended Data Figure 8b-j).

Finally, to solidify the mechanisms linking microbiome legacy to plant phenotype, we conducted a mediation analysis to determine whether the 198 genes that were differentially expressed depending on inoculum legacy (Figure 4a-b) were causally involved in trait responses to acute drought (Figure 4c). Expression patterns of this subset of genes were summarized in two dimensions (MDS1 and MDS2) using non-metric multidimensional scaling of Bray-Curtis dissimilarities among individual plants. MDS1 mediated 18.0% of the total drought-induced decrease in iWUE ($p < 0.001$), and 8.9% of the total decrease in transpiration ($p = 0.018$; Figure 4d). In contrast, MDS2 mediated 11% of the iWUE response to drought ($p = 0.03$), but in the opposite direction, meaning that the activity of these genes counteracted the negative effects of acute drought on iWUE. Four of the top eight genes with the strongest positive loadings on MDS2 were orthologs of the maize gene ZmNAS7, which encodes the enzyme nicotianamine synthase; two of these were also in the top 5% of genes with the strongest negative loadings on MDS1 (Extended Data Figure 9), indicating that they have a protective function that minimizes the drop in iWUE during acute drought. All four ZmNAS7 orthologs were up-regulated between 4-fold and 12-fold in response to drought, but only in plants that were inoculated with dry-legacy microbiota (Figure 4b, gene set IV), suggesting a possible mechanism by which microbiota with a legacy of chronic water stress confer improved drought tolerance. Consistent with this, salicylic acid–a key regulator of root microbiome assembly (Lebeis et al. 2015)–is reported to induce expression of ZmNAS7 (Zhou et al. 2013). Furthermore, although nicotianamine is best known for its role in metal transport, the overexpression of NAS genes in rice conferred tolerance of acute drought, including maintenance of photochemical efficiency at pre-drought levels (Lee et al. 2017).

Overall, these results support our hypothesis that microbiomes with a history of water stress improve gamagrass responses to drought. For instance, iWUE, which was higher in dry-legacy-inoculated plants (Figure 4e), measures the potential water cost of carbon assimilation (photosynthetic rate (A)/ stomatal conductance (gs)) and is an important component of plant drought tolerance. The traits that were negatively associated with dry-legacy microbiota likely also represent a beneficial response to acute drought because smaller metaxylem vessels could prevent embolisms (Klein et al. 2020), and smaller median root diameter may lower the energy cost of root growth and enable deeper soil exploration. We emphasize that these patterns represent averages across multiple independent soils within each legacy group, increasing

our confidence in their generalizability. In addition, these signatures of microbiota legacy on the plant transcriptome were detectable even when averaging across all treatments applied during the conditioning phase, suggesting that microbiome legacy effects with implications for plant fitness are robust to short-term perturbations. Altogether, our results show that a complete understanding of plant drought response requires consideration of the microbial environment, including legacy effects of water stress.

Beneficial microbiome drought legacy effects do not extend to a common crop, *Zea mays*

Additionally, to explore whether the observed microbial feedback effects were transferable across hosts, we simultaneously applied the same inocula to seedlings of the maize (*Zea mays* ssp. *mays*) genotype B73. Maize is closely related to gamagrass, making it a good candidate for testing whether microbiome legacy effects are transferable to domesticated, non-native species. Maize plants were four weeks old at the time of sampling, and the drought treatment was sufficient to significantly hinder maize growth (Extended Data Figure 10a).

Unlike in eastern gamagrass, the taxonomic composition of bacterial communities in maize crown roots retained clear signatures of the inoculum precipitation legacy (Extended Data Figure 10b., ANOVA.CCA, $F_{1,255}$=4.254, R^2=0.014, p=0.001), in addition to being impacted by acute drought treatment (Extended Data Figure 10c). Also unlike in gamagrass, test phase drought treatment significantly increased beta-dispersion compared to the well watered control, indicating that water deprivation gave rise to more variability in the maize microbiome (Extended Data Figure 10d; ANOVA $F_{1,262}$=18.17, p<0.001). Like in eastern gamagrass, however, all inocula resulted in root communities with a similar mean Shannon diversity (Extended Data Figure 10e). Next, we identified bacterial amplicon sequence variants (ASVs) that were differentially abundant in droughted *vs.* control plants in a manner that depended on the precipitation legacy of the microbiome. This included only two ASVs in gamagrass roots, ASV1598 (*Azospirillum* sp.) and ASV2352 (*Enterobacteriaceae*) (Extended Data Figure 11a), but 100 maize root ASVs (Extended Data Figure 11b), again indicating that gamagrass root microbiomes are more stable than those of maize. The maize ASV enrichments did not show a phylogenetic pattern. The ASVs identified in this analysis could contribute to plant phenotypic responses to drought.

We also characterized the transcriptional response of maize and found that 23 genes were up-regulated in plants inoculated with dry-legacy microbiota, relative to those that received wet-legacy inocula (Extended Data Figure 12a). These included six defense-related genes (particularly those related to jasmonic acid signaling), suggesting that soil microbiota from low-precipitation sites were perceived as pathogens by maize but not eastern gamagrass. Other notable functions that were up-regulated by the dry-legacy inocula in maize include root development and iron acquisition (Supplementary Data 1). We also identified 109 maize genes that responded to drought treatment in a manner that was dependent on microbial

precipitation legacy, of which only 30 were identified as drought-responsive when averaging across inocula (Extended Data Figure 12b). Like in eastern gamagrass, most of these were drought-responsive only in wet-legacy-inoculated or only in dry-legacy-inoculated plants, with relatively few genes reversing the direction of their drought response depending on inoculum legacy (Extended Data Figure 12c). For example, 30 genes were up-regulated in response to drought only in plants grown with wet-legacy microbiota (Extended Data Figure 12c, gene set I). These genes included several related to pathogen defense (Zm00001eb116230, Zm00001eb150050, Zm00001eb222540) and one involved in the response to symbiotic fungi (Zm00001eb033580), suggesting that soils from high-precipitation regions contain both harmful and beneficial microorganisms and that interactions with both types are activated under water deprivation in maize (Supplementary Data 1). Notably, one of the 18 genes that reversed its drought response depending on the inoculum was TIP3, which encodes an aquaporin that regulates water storage in the vacuole (Chaumont et al. 2001). Wet-legacy microbiota caused TIP3 expression to increase 7-fold during acute drought, whereas dry-legacy microbiota caused TIP3 expression to decrease nearly 3-fold (Extended Data Figure 12c, gene set VI). Averaged across the two inocula, however, TIP3 was not differentially expressed between droughted and well-watered plants; thus, its role in drought response was apparent only when accounting for microbiota legacy.

We identified four sets of orthologous genes that were sensitive to microbiota legacy in both host species. Zm00001eb076200 encodes a peroxidase that reversed its drought response depending on inoculum in maize; however its *T. dactyloides* ortholog, Td00002ba025285, was up-regulated 4-fold due to drought but only in plants grown with wet-legacy inoculum. The gene Zm00001eb077640, encoding L-allo-threonine aldolase, also reversed its drought response in maize. In contrast, its ortholog Td00002ba026366 was consistently up-regulated in response to drought, but more so in plants inoculated with dry-legacy biota. The maize pathogenesis-related protein-like gene Zm00001eb150050, which has been linked to both biotic and abiotic stress responses, was up-regulated 7-fold in response to drought only in plants inoculated with wet-legacy microbiota; however, both of its *T. dactyloides* orthologs were down-regulated 8-fold in plants inoculated with microbiota from low-precipitation sites, relative to inocula from high-precipitation sites, regardless of water availability. Finally, Zm00001eb301540 encodes a tryptophan synthase that was up-regulated 1.7-fold in the presence of wet-legacy but not dry-legacy microbes; its ortholog Td00002ba012570, in contrast, was down-regulated in the presence of wet-legacy microbes. Thus, none of these four genes showed congruent responses to drought in maize and eastern gamagrass.

Finally, we investigated whether the beneficial effects of microbiome legacy on *T. dactyloides* phenotype (Figure 4d-e) were also conferred on maize. Overall, microbiome precipitation legacy explained only 2.0% of the phenotypic variation in maize (Extended Data Figure 13a., ANOVA.CCA, $F_{1,175}$=3.72, R^2=0.02, p=0.001), a weaker effect than observed in eastern gamagrass. We found no evidence that dry-

legacy microbiota buffered maize plants from the phenotypic effects of drought stress as they did for *T. dactyloides*. In fact, root mass and iWUE s-indexes were slightly higher in maize inoculated with wet-legacy microbiomes than maize inoculated with dry-legacy microbiomes (Extended Data Figure 13b,c). This pattern is consistent with our observation that dry-legacy inocula induced higher expression of defense-related genes (Extended Data Figure 12a). We also found that several mineral nutrients in maize roots (Ni, Li, Sr, Cu, Co) were impacted by microbiome legacy (Extended Data Figure 13f,g,h,i,j), perhaps reflecting that the maize root microbiome heterogeneity causes increased variability in the root macro- and micro-nutrient profiles (Salas-González et al. 2021).

CONCLUSIONS

Although microbially-mediated legacy effects of past drought on current plant performance have been reported previously (de Vries et al. 2023; Evans, Allison, and Hawkes 2022), their molecular mechanisms have been largely unexplored until now. Numerous microbial genes and functional pathways, including those suggesting an increased nitrogen metabolizing and DNA repair capacity in dry-legacy microbiota, are associated with mean annual precipitation, a conclusion which we validated by controlling for other soil properties that influence microbial communities, namely soil porosity and mineral nutrient content. Furthermore, we confirmed that these metagenomic patterns are shared by two independent natural precipitation gradients separated by more than 7,000 km, suggesting that these signatures of historic precipitation levels may generalize to soils across the globe.

We show that these metagenomic precipitation legacies have significant implications for plant growth, beginning with altered transcription of host genes in the roots. In the prairie grass *Tripsacum dactyloides*, dry- and wet-legacy soil microbiomes give rise to taxonomically similar root endosphere communities yet have strikingly different effects on plant gene expression and phenotype. Indeed, root microbiome stability appears to play a role in adaptive plant responses to a subsequent acute drought, also suggesting that microbial physiological responses are likely as important or more important than taxonomic enrichments, which are more typically investigated. These effects were robust to a five-month perturbation, which could mimic a particularly dry or wet season. The differences in gamagrass and maize responses to microbiome history indicates that crops may not reap the same benefits as native plant species from potentially beneficial microbial communities, and warrant further study. Broadly, these findings significantly contribute to our understanding of microbiome drought legacy effects persistence and role in plant drought responses, with implications for agricultural and ecosystem management.

METHODS

Legacy phase: Characterization of soils across precipitation gradients

Study sites and collection of soils

Experimental input soil was collected from six never-irrigated native prairies across Kansas, USA in October 2020 and 2021. This includes Eastern Kansas tallgrass prairies: Welda Prairie (WEL), Clinton Wildlife Reserve (CWR), and Konza Wildlife Reserve (KNZ), as well as Western Kansas shortgrass prairies: Hays Prairie (HAY), Smoky Valley Ranch (SVR), and Kansas State University's Tribune Southwest Research Center (TRI). Each site was split into three subplots. In each subplot, the top ≈10 cm of surface soil and thick plant root masses were removed with a bleach sterilized metal shovel. Then, approximately 2.5 L of soil was collected and pooled into a ziplock bag, for a total of ≈7.5L of soil collected per site. Soil was held at room temperature for transport back to the laboratory where it was then stored at 4˚C.

Additional soil sampling was undertaken across 10 selected regions in Santiago Island, Cabo Verde in March 2022. Each field was divided into six equal parts (subplots). Within each subplot, six samples were collected following a typical zig-zag pattern with approximately 3 m of separation between the harvesting points and avoiding field edges, roads, and pathways. Soil samples were then collected from the top 10 cm layer using a handheld soil auger and pooled to produce a unique composite sample per subplot. Thus, for each soil, we collected 6 composite samples. All tools used for soil collection were previously disinfected with 70% ethanol, and the operators wore gloves the whole time. Soil samples were transported in clean plastic bags to Instituto Nacional de Investigação e Desenvolvimento Agrário (INIDA), where they were air-dried in sterile plastic trays at room temperature for 1 week and then sieved using a 2 mm sieve. Soil samples were stored at 4 ºC until use.

Precipitation data extraction

To characterize precipitation conditions in Kansas and Santiago Island, precipitation parameters were retrieved from publicly available sources with global coverage. Briefly, for Kansas, daily precipitation for the period 1981 to 2021 was extracted from the NASA POWER database (Zhang et al. 2008) based on the latitude and longitude of each region. For Santiago Island, we compiled precipitation data from (Sanchez-Moreno, Mannaerts, and Jetten 2014).

Soil elemental content and pH analysis

The soil elemental content was determined by using ICP-MS. The soil samples were first dried using plastic weighing boats in the fume hood for approximately 72h at room temperature. Five grams of soil was then weighted in 50 mL Falcon tubes with a four-decimal balance, and digested with 20 mL of 1 M NH_4HCO_3, 5 mM diamine-triamine-penta-acetic acid (DTPA), and 5 mL 18.2 MΩcm Milli-Q Direct water (Merck Millipore), 1h at 150 rpm in a rotary shaker (adapted from Soltanpour and Schwab (Soltanpour and Schwab 1977)). Each sample was gravity filtered through a quantitative filter paper (Whatman 42- WHA1442070) until obtaining approximately 5 mL of filtrate. Prior to the digestion, 20 µg/ L of Indium (In) was added to the nitric acid Primar Plus (Fisher Chemicals) as an internal standard for assessing error in dilution, variations in sample introduction and plasma stability in the ICP-MS instrument. 0.5mL of the soil filtrates were then open-air digested in Pyrex tubes using 1 mL of concentrated trace metal grade nitric acid spiked indium internal standard for 2h at 115 ºC in dry block heater (DigiPREP MS, SCP Science; QMX Laboratories, Essex, UK). After cooling down, the digests were diluted to 10 ml with 18.2 MΩcm Milli-Q Direct water and elemental analysis was performed using an ICP-MS, PerkinElmer NexION 2000 equipped with Elemental Scientific Inc 4DXX FAST Dual Rinse autosampler, FAST valve and peristaltic pump. The instrument was fitted with PFA-ST3 MicroFlow nebulizer, baffled cyclonic C3 high sensitivity glass spray chamber cooled to 2ºC with PC3X Peltier heated/cooled inlet system, 2.0 mm i.d. quartz injector torch and a set of nickel cones. Twenty-four elements were monitored including following stable isotopes: ^{7}Li, ^{11}B, ^{23}Na, ^{24}Mg, ^{31}P, ^{34}S, ^{39}K, ^{43}Ca, ^{52}Cr, ^{55}Mn, ^{56}Fe, ^{59}Co, ^{60}Ni, ^{63}Cu, ^{66}Zn, ^{75}As, ^{82}Se, ^{85}Rb, ^{88}Sr, ^{98}Mo, ^{111}Cd, ^{208}Pb and ^{115}In. Helium was used as a collision gas in Kinetic Energy Discrimination mode (KED) at a flow rate of 4.5 mL/ min while measuring Na, Mg, P, S, K, Ca, Cr, Mn, Fe, Ni, Cu, Zn, As, Se and Pb to exclude possible polyatomic interferences. Remaining elements were measured in the standard mode. Any isobaric interferences were automatically corrected by the instrument Syngistix™ software for ICP-MS v.2.3 (Perkin Elmer). The ICP-MS measurements were performed in peak hopping scan mode with dwell times ranging from 25 to 50 ms depending on the element, 20 sweeps per reading and 3 replicates. The ICP-MS conditions were as follows: RF power – 1600 Watts, auxiliary gas flow rate 1.20 L/ min. Torch alignment, nebuliser gas flow and quadrupole ion deflector (QID) voltages (in standard and KED mode) were optimized before analysis for highest intensities and lowest interferences (oxides and doubly charged ions levels lower than 2.5%) with NexION Setup Solution containing 1 µg/ L of Be, Ce, Fe, ln, Li, Mg, Pb and U in 1% nitric acid using a standard built-in software procedure. To correct for variation between and within ICP-MS analysis runs, liquid reference material was prepared using pooled digested samples, and run after the instrument calibration, and then after every nine samples in all ICP-MS sample sets. Equipment calibration was performed at the beginning of each analytical run using seven multi-element calibration standards (containing 2 µg/L In internal standard) prepared by

diluting 1000 mg/L single element standards solutions (Inorganic Ventures; Essex Scientific Laboratory Supplies Ltd) with 10% nitric acid. As a calibration blank, 10% nitric acid containing 2 µg/L In internal standard was used and it was run throughout the course of the analysis.

Sample concentrations were calculated using the external calibration method within the instrument software. Further data processing including calculation of final elements concentrations was performed in Microsoft Excel. First, samples set that have been run at different times were connected as an extension of the single-run drift correction. Linear interpolation between each pair of liquid reference material standards was used to generate a theoretical standard for each sample that was then used to correct the drift by simple proportion to the first liquid reference material standard analyzed in the first run. Liquid reference material composed of pooled samples was used instead of the CRM to match the chemical matrix of the samples as closely as possible, thereby emulating the sample drift. Second, the blank concentrations were subtracted from the sample concentrations and then each the final element concentrations were obtained by multiplying by the dilution factor and normalizing the elements concentrations to the samples dry weight.

Metagenomic analysis of free-living soil microbes

DNA extraction

To determine the taxonomic composition and genomic content of the collected soils' microbial communities, approximately 5 g of each soil were transferred into 50-mL falcon tubes containing 20 mL of sterile distilled water. To remove large plant debris and soil particles, the samples were shaken thoroughly and filtered using 100-µm nylon mesh cell strainers into new sterile 50-mL tubes. The filtered solutions were centrifuged at high speed for 20 min in a centrifuge Eppendorf 5810R and most of the supernatants were discarded. The remaining 1-2 mL of supernatants were used to dissolve the pellets, and the resulting suspensions were transferred to sterile 1.5-mL Eppendorf tubes. Samples were centrifuged again at high speed in a benchtop centrifuge and the supernatants were discarded. The remaining pellets were stored at -80 ºC until DNA extraction. For the DNA extraction we used 96-well-format MoBio PowerSoil Kit (MOBIO Laboratories; Qiagen) following the manufacturer's instructions. Before starting the extraction, all samples were randomized by placing them in a plastic bag that was shaken several times. Samples were then taken individually from the bag and loaded in the DNA extraction plates. This random distribution was maintained throughout library preparation and sequencing.

Metagenomic library preparation and sequencing

DNA sequencing libraries were prepared using the Rapid PCR Barcoding Kit (SQK-RPB004) from Oxford Nanopore Technologies, UK. In brief, 1 µL Fragmentation Mix (FRM) was added to 3 µL DNA

(2-10 ng/µL), and the reaction was mixed by gently finger-flicking. The DNA was fragmented using the following conditions: 30°C for 1 min, then 80°C for 1 min in an Applied Biosystems Veriti 96-Well Thermal Cycler (Applied Biosystems, CA, USA). The fragmented DNA was cooled, then barcoded and amplified in a PCR reaction containing 20 µL nuclease-free water, 25 µL LongAmp Taq 2X master mix (New England Biolabs, MA, USA), 4 µL fragmented DNA, and 1 µL barcode adaptor. The reaction was gently mixed and amplified using the following conditions: 95°C for 3 min, 20 cycles of denaturation at 95°C for 15 s, annealing at 56°C for 15 s and extension at 65°C for 6 min, and a final extension of 65°C for 6 min. The resulting DNA library was purified using 0.6X Agencourt AMPure XP beads (Beckman Coulter, CA, USA) and eluted in 10 µL 10 mM Tris-HCl pH 8.0, 50 mM NaCl. The library concentration was determined using a Qubit 4 Fluorometer with the Qubit dsDNA HS Assay Kit (Thermo Fisher Scientific, USA). Equimolar quantities of individual barcoded sample libraries were pooled and the volume adjusted to 10 µL using 10 mM Tris-HCl pH 8.0, 50 mM NaCl. Subsequently, 1 µL RAP was added to the pooled library and the tube was incubated at room temperature for 5 min. Then, 34 µL Sequencing Buffer, 25.5 µL Loading Beads, and 4.5 µL nuclease-free water were added to the tube, and the contents were mixed gently. The prepared pooled library was added to a verified and primed FLO-MIN106 R9.4.1 flow cell (Oxford Nanopore Technologies, UK) in a MinION (Oxford Nanopore Technologies, UK) following the manufacturer's instructions. DNA sequencing was conducted with default parameters using a MinIT (Oxford Nanopore Technologies, UK) with MinKNOW v2.1.12 (Oxford Nanopore Technologies, UK). Fast5 files were base-called with Guppy v4.0.15 using the template_r9.4.1_450bps_hac.jsn high accuracy model (Oxford Nanopore Technologies, UK).

Metagenomic sequence processing and analysis of soil metagenome content

The initial dataset underwent demultiplexing, and primer and barcode sequences were trimmed using qcat v1.1.0 (Oxford Nanopore Technologies Ltd., UK). Reads with ambiguous barcode assignments were excluded from further analysis. The reads were filtered with NanoFilt v2.8.0 (De Coster et al. 2018) to discard low quality sequences (Q-score < 9) and sequences < 100 bp. We used the Kraken v2.1.2 pipeline (Wood, Lu, and Langmead 2019) for classifying the whole metagenome shotgun sequencing reads. The reads were classified using the Kraken 2 archaea, bacteria, viral, plasmid, human, UniVec_Core, protozoa and fungi reference database (k2_pluspf_20220607). To estimate relative abundances, the Bracken v2.7 pipeline (Lu et al. 2017) was applied to the classification results. Subsequently, Pavian v1.0 (Shamimuzzaman et al. 2020) facilitated the extraction of abundance and taxonomic tables.

Enrichment of bacteria biological functions associated with precipitation gradients

To identify metabolic processes that were enriched within the microbial communities, the sequence reads were assembled into contigs for each sample using metaFlye (Kolmogorov et al. 2020) from the Flye v2.9 package with default mode. The contigs generated were then grouped and deduplicated using the dedupe.sh tool in BBTools v38.76 v3.4.0 ("BBTools" 2016) to eliminate redundancies. Next, we determined the relative abundance of the contigs by mapping the reads from the samples to the contigs using minimap2 v2.17 (Li 2018), and extracting the relative abundance counts using CoverM v0.6.1 (https://github.com/wwood/CoverM) in the 'contig' mode and reads_per_base coverage method. Taxonomic classification of the contigs was performed using the CAT v8.22 taxonomic classification pipeline (von Meijenfeldt et al. 2019). Subsequently, the contigs were filtered to retain only bacteria sequences. DESeq2 v1.40.0 (Love, Huber, and Anders 2014) was utilized to determine the contig enrichment profiles by fitting a generalized linear model (GLM) with the following design:

$$\text{Abundance} \sim \text{Legacy} + \text{Replicate}$$

Drought legacy soil vs precipitation legacy soil comparison was extracted from the fitted model. Contigs meeting the criteria of an FDR-adjusted p-value (q-value) < 0.05 and a $\log_2$-transformed fold change > 2 were selected for further analysis. Open reading frames encoded within the contigs were predicted using FragGeneScanRs v1.1.0 (Van der Jeugt, Dawyndt, and Mesuere 2022) with default settings. This was followed by functional annotation of the predicted proteins using the eggNOG-mapper v2.1.9 (Cantalapiedra et al. 2021) pipeline with the eggNOG v5.0.2 database (Huerta-Cepas et al. 2019) with Diamond v2.0.11 (Buchfink, Reuter, and Drost 2021) and MMseqs2 (Steinegger and Söding 2017). The genes annotated with Gene Ontology (GO) classifications were subsequently extracted, and a GO enrichment analysis focusing on biological processes was conducted. This involved employing adaptive GO clustering in conjunction with Mann–Whitney U testing, utilizing the GO_MWU tool as described by (Wright et al. 2015). In this analytical approach, genes were ranked based on the signed $\log_2$-transformed fold change values. Significantly enriched and depleted GO categories were determined by an adjusted p-value of < 0.05. The most prominent enriched and depleted GO categories shared across comparisons were visualized in ggplot2 v3.4.2 and coloured based on the square root transformed delta rank values (enrichment score) of the GO categories.

Conditioning phase: Assessing the robustness of functional precipitation legacy effects to short-term perturbations

Experimental design and sample collection

The soils used during the conditioning phase and subsequent experiments were the same that were collected from across the Kansas precipitation gradient, as described above in Legacy phase: Characterization of soils across precipitation gradients. The conditioning phase took place over ≈20 weeks at the University of Kansas from December 17th, 2020 to May 5th, 2021. Each of the six input soils remained independent throughout the experiment. Mesocosms consisted of a 1:1 (v/v) mixture of field collected soil to sterile turface MVP (Turface Athletics, Buffalo Grove, IL). A total of 192 sterile 100 mL pots were filled with one of the six 1:1 soil mixtures, which were then subjected to four conditions in a fully-factorial design: with or without a host, and either water-stressed or well-watered. Thus, 48 soil mesocosms total, and 12 mesocosms per individual soil, were exposed to each of the four conditions. Half the pots were planted with seedlings of the native prairie grass *T. dactyloides* (Eastern gamagrass, cultivar "Pete"); the rest remained unplanted. All mesocosms were allowed to adapt to their watering regimes in a growth chamber set to a 12-hour day cycle, 27°C/23°C, and ambient humidity. Well-watered control pots were watered every 1-2 days and water-stressed plants were watered every 3-5 days, when plants displayed drought symptoms (e.g., leaf curling). All pots were fertilized with 35 ml of 1mL/L concentration of Bonide 10-10-10 plant food (Bonide Products LLC, Oriskany, NY) on week 8 and week 12. To characterize the baseline microbial communities going into the conditioning treatments, we sampled four replicates of each soil/treatment combination one week after the start of the conditioning phase. The top centimeter of soil was discarded and the remaining soil was homogenized to ensure even sampling of the top, middle, and bottom of the pot. Two grams of this homogenized soil were placed in a 15mL tube, flash-frozen in liquid nitrogen, and stored at -80°C for microbial DNA and RNA extraction. An additional 6g of homogenized soil were preserved in 50 mL conical tubes for downstream use as inocula during the test phase. To characterize the effects of the four treatments on the microbial communities, we sampled all remaining replicates at the end of the 20-week conditioning phase. Soil samples were collected as described for the baseline communities. Additionally, for the planted pots, we measured *T. dactyloides* shoot height before uprooting the plants. We collected samples of a crown root from each plant (3 cm long each, beginning 2 cm from the base of the plant) and stored them in 50% ethanol at 4˚C for downstream LAT analysis. The remaining roots and shoots were dried in an oven at 225˚C for 12 hours and then weighed separately.

Sequencing post-conditioning metagenomes

Total DNA was extracted from baseline and post-conditioning soil sub-samples using the DNA Set for NucleoBond RNA Soil Kit (Macherey-Nagel, Düren, Germany) according to the manufacturer's instructions. Subsequently, DNA sequencing libraries were prepared using the Rapid PCR Barcoding Kit (SQK-RPB004) from Oxford Nanopore Technologies, UK, and sequenced on a FLO-MIN106 R9.4.1 flow cell (Oxford Nanopore Technologies, UK) in a MinION (Oxford Nanopore Technologies, UK), with a MinIT (Oxford Nanopore Technologies, UK) using MinKNOW v2.1.12 (Oxford Nanopore Technologies, UK) as described before. Raw sequence data were demultiplexed and primer and barcode sequences were trimmed using qcat v1.1.0 (Oxford Nanopore Technologies Ltd., UK). Reads with ambiguous barcode assignments were excluded from further analysis. The reads were filtered with NanoFilt v2.8.0(De Coster et al. 2018) to discard low quality sequences (Q-score < 9) and sequences < 100 bp. We used the Kraken v2.1.2 pipeline (Wood, Lu, and Langmead 2019) for classifying the whole metagenome shotgun sequencing reads. The reads were classified using the Kraken 2 archaea, bacteria, viral, plasmid, human, UniVec_Core, protozoa and fungi reference database (k2_pluspf_20220607). To estimate relative abundances, the Bracken v2.7 pipeline (Lu et al. 2017) was applied to the classification results. Subsequently, Pavian v1.0 (Breitwieser and Salzberg 2020) facilitated the extraction of abundance and taxonomic tables. Functions in phyloseq v1.44.0 (McMurdie and Holmes 2013) with microbiome v1.22.0 and microbiomeutilities v1.0.17 (Shetty 2023) were used to filter the dataset and remove samples with low read depth (<1000 reads), remove unidentified taxa and singletons, transform abundance values using rarefaction, subset and merge sample and taxonomic groups and perform other dataframe manipulations. To assess the alpha diversity across the samples, we calculated the Shannon Diversity Index using phyloseq v1.44.0. We used ANOVA to test for significant differences in Shannon Diversity indices between groups and means were separated using Tukey's honestly significant difference (HSD) test from the agricolae v1.3.5 R package (Mendiburu 2019). For beta-diversity, Bray-Curtis dissimilarity matrices were calculated using phyloseq v1.44.0 "bray" method and the variance explained by legacy, conditioning, and host were estimated by performing permutational multivariate analysis of variance (PERMANOVA) using the adonis2 function in vegan v2.6.4 R package (Oksanen et al. 2007). Constrained ordination of beta-diversity was plotted using canonical analysis of principal coordinates (CAP) based on Bray-Curtis dissimilarity matrices calculated with vegan v2.6.4. We visualized differences with the CAP analysis, using the model:

$$\sim \text{legacy} + \text{Condition (conditioning} + \text{host} + \text{replicate)}$$

The relative abundance of taxa was plotted as a stacked bar representation using phyloseq v1.44.0. The tax_glom function in phyloseq v1.44.0 was used to agglomerate taxa, and the aggregate_rare function

in microbiome v1.22.0 was used to aggregate rare groups. We used DESeq2 v1.40.0 to calculate the enrichment profiles by fitting a generalized linear model (GLM). We extracted the following comparisons from the fitted model for each soil legacy separately: wet legacy baseline (input community) vs. wet-legacy watered, wet-legacy-droughted, dry-legacy, dry-legacy watered, and dry legacy-droughted. Taxa were considered significant if they had an FDR-adjusted p-value (q-value) < 0.05. The results of the GLM analysis were rendered in heatmaps, coloured based on the $\log_2$-transformed fold change output by the GLM. Significant differences between comparisons with a q-value < 0.05 with $\log_2$-transformed fold change > 2 were highlighted with black squares.

To identify enriched metabolic processes within the microbial communities, the sequence reads from individual samples were assembled into contigs, their relative abundance counts determined, and were subjected to taxonomic classification as described before. DESeq2 v1.40.0 was utilized to determine the bacterial contig enrichment profiles by fitting a generalized linear model (GLM). We extracted the following comparisons from the fitted model: wet legacy baseline (input community) vs. wet-legacy watered, wet-legacy-droughted, dry-legacy, dry-legacy watered, and dry legacy-droughted. Contigs meeting the criteria of an FDR-adjusted p-value (q-value) < 0.05 and a $\log_2$-transformed fold change > 2 were selected. Open reading frames were predicted and functionally annotated, and genes with GO classifications were subjected to GO enrichment analysis with the GO_MWU tool (Wright et al. 2015).

Root system architecture and root biomass

A Perfection V600 flatbed scanner (Epson, Nagano, Japan) was used to scan intact root systems collected from test phase plants. The scanner was set to professional mode, reflective, document, black and white mode, 600 dpi, with a threshold of 55. A clear plastic tray with enough DI water to cover the entire bottom of the tray was placed on the scanning bed. For each sample, the root system was placed in the tray with water and the tangled roots were gently pulled apart and spread across the tray with plastic tweezers until roots were no longer overlapping. A small amount of fine fibrous roots that fell off during this process were pushed to the corner of the tray and not included in the root cluster scan. The scanned root images were then analyzed using Rhizovision Explorer software in “whole root” mode and converted to 600 dpi (Seethepalli et al. 2021). The region of interest tool was used to outline the main root bundle before collecting feature measurements. After collection of root system architecture data, the roots were dried in an oven at 225˚C for 12 hours and then weighed.

Root Laser Ablation Tomography (LAT) analysis

We collected samples of a crown root from each plant (3 cm long each, beginning 2 cm from the base of the plant) and stored them in 50% ethanol at 4˚C. The samples were shipped to the University of Nottingham for downstream LAT analysis. Briefly, root segments were dried with an automated critical point dryer (CPD, Leica EM CPD 300, Leica Microsystem). Then, samples were ablated by a laser beam (Avia 7000, 355 nm pulsed laser) to vaporize the root tissue at the camera focal plane ahead of an imaging stage. Then, cross-sectional images were taken using a Canon T3i camera with a 5×micro-lens (MP-E 65 mm) on the laser-illuminated surface. ImageJ software was used to measure root anatomical traits captured in the high-quality LAT images.

Analysis of gamagrass morphological features during conditioning phase

To identify morphological features in gamagrass that changed with the conditioning (drought and well water) treatments, we analyzed the Root Laser Ablation Tomography (LAT) datasets (average area aerenchyma, number aerenchyma, number metaxylem, cortical cell layers, total area metaxylem, average area metaxylem, stele min. diameter, stele max. diameter, stele area, stele perimeter, total area aerenchyma, adjusted cortex area, root min. diameter, cortex min. diameter, root max. diameter, cortex max. diameter, total perimeter, cortex perimeter, root total area, cortex area) for gamagrass as well as other plant features (root shoot ratio, number of leaves, number of green leaves, root mass, shoot mass, shoot height, shoot height in pot) for differences. For each feature, we used ANOVA to test for significant differences between groups and means were separated using Tukey's honestly significant difference (HSD) test from the agricolae v1.3.5 R package. Subsequently, the feature values were normalized using the rescale function from the scales v1.2.1 R package. The mean normalized feature values were then visually represented on a heatmap using ggplot2 v3.4.2. Subsequently, Pearson correlation coefficients and corresponding p-values between these features were computed using the rcorr function from the Hmisc v5.0.1 package. The results of the correlation analysis were graphically presented using ggplot2 v3.4.2, where the color of the plots reflected the correlation coefficient values. Significant correlations ($p < 0.05$) were emphasized with black squares on the plots. Furthermore, the coefficient of variation for the feature values was calculated and depicted using ggplot2 v3.4.2. The 3 plots were integrated based on the hierarchical clustering of the Pearson correlation coefficients of the features. The clustering employed the ward.D2 method within the hclust function in R, utilizing Euclidean distances calculated using the dist function. For each cluster identified, we selected the feature with the highest coefficient of variation as a representative for the cluster.

Metatranscriptome library preparation and sequencing

Total RNA was extracted from baseline and post-conditioning soil sub-samples using the NucleoBond RNA Soil Kit (Macherey-Nagel, Düren, Germany) using the manufacturer's instructions. Isolated RNA was treated with Turbo DNA-free (Applied Biosystems, Waltham, MA, USA) to remove contaminating DNA, following the manufacturer's instructions. Subsequently, RNA libraries were prepared using 1 µg of RNA according to established protocols with modifications. Briefly, poly(A)-tail-containing RNA was removed from the samples using Sera-mag oligo(dT) magnetic beads (GE Healthcare Life Sciences, Marlborough, MA, USA) and then ribodepleted with the NEBNext rRNA Depletion Kit (New England Biolabs, MA, USA), following the manufacturers' instructions. The RNA was eluted with a fragmentation mix consisting of 6.25 µL Milli-Q water, 5 µL 5X First strand buffer, and 1.25 µL random primers (3 µg/µL) and fragmented at 94°C for 6 min. First-strand cDNA synthesis was performed using a mixture of 0.8 µL reverse transcriptase, 2 µL 100 mM DTT, 0.4 µL 25 mM dNTP, 0.5 µL RNAseOUT (40U/µL), 10 µL RNA, and 6.3 µL Milli-Q water. The reactions were incubated at 25°C for 10 min, 42°C for 50 min, and 70°C for 15 min. Second-strand cDNA synthesis was performed by adding a master mix of 18.4 µL Milli-Q water, 5 µL 10X second strand buffer, 1.2 µL 25 mM dNTP, 0.4 µL RNAse H (5U/µL), and 5 µL DNA Pol I (10U/µL) to the sample, followed by incubation at 16°C for 1 h. The samples were then purified using Agencourt AMPure XP beads. Subsequently, the libraries were end-repaired with a mixture of 30 µL sample, 2.5 µL of 3 U/µL T4 DNA polymerase, 0.5 µL of 5 U/µL Klenow DNA polymerase, 2.5 µL of 10 U/µL T4 PNK, 5 µL of 10X T4 DNA ligase buffer with 10 mM ATP, 0.8 µL of 25 mM dNTP mix, and 8.7 µL Milli-Q water, incubated at 20°C for 30 min, and purified again using Agencourt AMPure XP beads. Following this, the RNA libraries were adenylated in a mix containing 34 µL of the end-repaired sample, 3 µL of 5 U/µL Klenow exo-, 5 µL of 10X Enzymatics Blue Buffer, 1 µL of 10 mM dATP, and 9 µL of Milli-Q water. The mixture was incubated at 37°C for 30 min, followed by 70°C for 5 min, and then purified using Agencourt AMPure XP beads. Individual samples were indexed through ligation using a mix of 10.25 µL sample, 1 µL of 600 U/µL T4 DNA ligase, 12.5 µL of 2X Rapid Ligation Buffer, and 1.25 µL of 2.5 µM indexing adapter from the KAPA Dual-Indexed Adapter Kit (Kapa Biosystems, MA, USA). The samples were incubated at 25°C for 15 min, followed by the addition of 5 µL of 0.5 M EDTA pH 8. The libraries were purified twice with Agencourt AMPure XP beads. The libraries were enriched in a reaction containing 20 µL sample, 25 µL of 2X KAPA HiFi HS Mix (Kapa Biosystems, MA, USA), 2.5 µL of 5 µM I5 primer, and 2.5 µL of 5 µM I7 primer. The reactions were initially heated to 98°C for 45 seconds, followed by 14 cycles of 98°C for 15 seconds, 60°C for 30 seconds, and 72°C for 30 seconds, with a final extension at 72°C for 1 minute. The resulting RNA libraries were purified using Agencourt AMPure XP beads, quantified on a Qubit 4 Fluorometer (Thermo Fisher Scientific, USA), and

the library size was assessed using High Sensitivity D1000 ScreenTape on the Agilent 4200 TapeStation (Agilent Technologies, Santa Clara, CA). Equimolar quantities of individual barcoded RNA libraries were pooled in a randomized manner and shipped on dry ice to Beijing Genomics Institute (BGI, Shenzhen, China). Each library pool was sequenced on an MGI Tech MGISEQ-2000 sequencing platform to generate a minimum of 10 million 100 bp paired-end reads per sample.

Metatranscriptome sequence processing and analysis

Cutadapt v4.6 (Martin 2011) as used to remove primer and barcode sequences, as well as low-quality sequences, from the paired-end reads of the sequenced RNA libraries. To identify taxa with enriched gene expression activity, the reads were classified using the Kraken v2.1.2 pipeline (Wood, Lu, and Langmead 2019) with the archaea, bacteria, viral, plasmid, human, UniVec_Core, protozoa and fungi reference database (k2_pluspf_20220607) and Bracken v2.7 pipeline (Lu et al. 2017) was applied to the classification results to estimate the relative abundances. The counts table was generated from Pavian v1.0 (Breitwieser and Salzberg 2020). Data filtering and statistical analysis was then performed as before using phyloseq v1.44.0 (McMurdie and Holmes 2013) with microbiome v1.22.0 and microbiomeutilities v1.0.17 (Shetty 2023).

Subsequently, the high-quality filtered reads were de novo assembled into a reference metatranscriptome using Trinity v2.15.1 (Grabherr et al. 2011) with default parameters. Open reading frames in transcripts were predicted with TransDecoder v5.7.1 with default settings. Functional annotation of the predicted proteins was performed using the eggNOG-mapper v2.1.9 (Cantalapiedra et al. 2021) pipeline, utilizing the eggNOG v5.0.2 database (Huerta-Cepas et al. 2019) with Diamond v2.0.11 (Buchfink, Reuter, and Drost 2021) and MMseqs2 (Steinegger and Söding 2017). The taxonomic classification of transcripts was conducted using the CAT v8.22 taxonomic classification pipeline (von Meijenfeldt et al. 2019). Sequence reads were further filtered using SortMeRNA v4.3.6 (Kopylova, Noé, and Touzet 2012) with the smr_v4.3_default_db.fasta database to remove residual amplified rRNA sequences. Transcript quantification analysis was performed using Salmon v1.10.0 (Patro et al. 2017) in the mapping-based mode with the de novo assembled reference metatranscriptome. Subsequently, the transcript-level abundance estimates from salmon were extracted in transcript per million (TPM) for the identified transcripts was utilized to determine the bacterial transcript enrichment profiles by fitting a generalized linear model (GLM) with the following design:

$$\text{Abundance} \sim \text{Legacy} + \text{Conditioning} + \text{Host} + \text{Replicate}$$

We extracted the following comparisons from the fitted model: water conditioning vs baseline, drought conditioning vs baseline, water conditioning with host vs baseline, drought conditioning with host vs baseline. This was done separately for each soil legacy. Genes meeting the criteria of an FDR-adjusted *p*-value (*q*-value) < 0.05 and a $\log_2$-transformed fold change > 2 were selected for further analysis. The genes annotated with Karyotic Orthologous Groups (KOG) classifications were used for KOG enrichment analysis with the KOGMWU v1.2 (Dixon et al. 2015) R package. For the analysis, genes were ranked based on the signed $\log_2$-transformed fold change values. Significantly enriched and depleted KOG categories were determined by an adjusted p-value of < 0.05. The most prominent enriched and depleted KOG categories shared across comparisons were visualized in ggplot2 v3.4.2 and coloured based on the square root transformed delta rank values (enrichment score) of the KOG categories.

Testing the implications of soil microbiome legacy on plants during subsequent acute drought

Experimental design and non-destructive phenotypic measurements

At the end of the Conditioning Phase, homogenized soil was collected from each pot by discarding the top one centimeter of soil, mixing the soil in the pot with a clean plastic spatula, and placing six grams in a sterile 50 mL conical tube. For rhizosphere samples (*i.e.,* planted pots), plants were gently pulled from the pots and the soil particles adhered to and within the root bundle were shaken into a sterile 50 mL conical tube. The rhizosphere particles were homogenized with a clean plastic spatula and particles were poured out of the tube until six grams remained. Soil and rhizosphere samples were stored at 4˚C overnight.

Soil microbes were extracted from the 6 gram soil or rhizosphere sample the following day by adding 25 mL of autoclaved 1X PBS with 0.0001% Tween-89 to the 50 mL tube containing the sample. Tubes were vigorously shaken to mix and break up large soil aggregates. Large particles were allowed to settle to the bottom of the tube; the supernatant was then filtered through autoclaved Miracloth (Sigma-Aldrich) into a new sterile 50 mL conical tube. Filtered samples were then centrifuged at 3600g for 25 mins at 4˚C. The supernatant was discarded and the microbial pellet was resuspended in 6mL of 1X PBS buffer using a vortex. The resuspended pellets were stored at 4˚C until used for inoculations a few hours later.

The microbial extract from each of the 192 Conditioning Phase pots (as well as the 24 uninoculated control pots) was used to inoculate 4 pots for the Test Phase: one pot per combination of watering treatment (droughted or control) and host species (maize or gamagrass). To create the inoculum, the resuspended pellet was inverted three times to mix and 1 mL of the sample was added to 100 mL of sterile 0.5X MS liquid medium, for a microbial titer equivalent to 0.01 g soil per mL. Finally, 25 mL of this suspension was inoculated onto the soil surface of each Test Phase pot. Thus, each extracted community from the conditioning phase was maintained as an independent replicate in the Test Phase. Before inoculation, pots

were planted with 3-4 day old gamagrass or maize germinants. Gamagrass seeds were soaked in 3% hydrogen peroxide for 24 hours and germinated in seed trays filled with sterile clay. Maize seeds were soaked in 70% ethanol for 3 minutes, then soaked in 5% NaClO on a rotator for 2 minutes, and then rinsed with sterile DI water three times. Treated maize seeds were germinated on sterile damp paper towels inside sealed plastic bags.

Pots were fully randomized and, prior to inoculation, were filled with a homogenized 5:1 (w/w) mixture of all-purpose sand (TechMix All-purpose 110241 from Menards) and calcined clay (Pro's choice rapid dry) that had been sterilized by autoclaving on a one hour liquid cycle. Pots were autoclaved on a 30 minute liquid cycle to sterilize and filled with the sand:clay mixture, leaving one inch of room at the top or the pot. To help keep the mixture from falling out of the drain holes in the bottom of the pots, a sterile filter paper was shaped into a cone, pushed to the bottom of the pot, and a sterile marble was used to weigh the paper down. This effectively blocked the substrate, but still allowed water to exit the drainage holes. Plants were grown under 12-hr days, 27°C/23°C (day/night), and ambient humidity, with the light setting set to 1, which is equivalent to 312 µmol/m2s. Three-way old gamagrass and maize leaf photosynthetic rates and gas exchange were measured using the LI-6800 (LI-COR, Lincoln, NE, USA), across 3-days for each host. The LI-6800 aperture was 2 cm, warmup tests were performed at the start of each measurement session, the Fluorometry was set to on, the APD_Leaf to set to 1.5 kpa. The newest, fully emerged leaf, which was most commonly the 4th leaf, on each plant was clamped in the chamber and allowed to stabilize until all measurements were stable for at least 30 secs before the measurements were recorded, which took approximately five minutes per leaf. Similarly, the leaf chlorophyll content was also measured using the MC-100 Chlorophyll Concentration Meter (apogee instruments, Logan, UT, USA).

Maize plants were sampled four weeks after planting and gamagrass was sampled five weeks after planting. In total, we measured 286 *T. dactyloides* plants (192 droughted, 94 well-watered) and 268 maize plants (182 droughted, 86 well-watered). At the end of the Test Phase, uprooted plants were gently shaken to remove the soil attached to roots, prior to the collection of phenotypic, transcriptomic, and microbiome data as described below. Plants were pulled from the pots and the soil attached to the roots were shaken off. One crown root was cut off with a ceramic blade and placed in a 1.7 mL tube on dry ice for downstream amplicon library preparation. Another crown root (0.15-0.2 g) was cut off with a ceramic blade, placed in a 1.7 mL tube, and flash frozen in liquid nitrogen for downstream RNA extraction. In between plants, the ceramic blade, plastic tweezers, plastic cutting board, and gloves were cleaned with 30% bleach. All samples were held on dry ice and then transferred to a -80˚C freezer for storage. Next, the root and shoot were separated with a ceramic blade. Three cm of crown root beginning ~2 cm from the base of the shoot was cut with a ceramic blade and submerged in 50% EtOH for LAT analysis. The rest of the root system was submerged in 70% EtOH in a 50 mL centrifuge tube for downstream root architecture scanning. Shoot

height and number of leaves were recorded. Shoots were placed in individual paper bags, dried in an oven at 225˚C for 12 hours, and the shoot dry weight was recorded.

Root system architecture and root biomass analyses

A Perfection V600 flatbed scanner (Epson, Nagano, Japan) was used to scan intact maize and gamagrass root systems collected from test phase plants. The scanner was set to professional mode, reflective, document, black and white mode, 600 dpi, with a threshold of 55. A clear plastic tray filled with clean water was placed on the scanning bed. Each root system was placed in the tray with water and the tangled roots were gently pulled apart using plastic tweezers until they were no longer overlapping. A small amount of fine fibrous roots that fell off during this process were pushed to the corner of the tray and not included in the root cluster scan. The scanned root images were then analyzed using Rhizovision Explorer software in "whole root" mode and converted to 600 dpi. The region of interest tool was used to outline the main root bundle before pressing play to collect feature measurements. Finally, after collection of root system architecture data, the roots were dried in an oven at 225˚C for 12 hours and then weighed.

Root Laser Ablation Tomography (LAT) analysis

We collected one crown root from each plant (3 cm long each, beginning 2 cm from the base of the plant) and stored them in 50% ethanol at 4˚C. These samples were shipped to the University of Nottingham for LAT analysis. Briefly, root segments were dried with an automated critical point dryer (CPD, Leica EM CPD 300, Leica Microsystem). Then, samples were ablated by a laser beam (Avia 7000, 355 nm pulsed laser) to vaporize the root tissue at the camera focal plane ahead of an imaging stage. Then, cross-sectional images were taken using a Canon T3i camera with a 5×micro-lens (MP-E 65 mm) on the laser-illuminated surface. ImageJ software was used to measure root anatomical traits captured in the high-quality LAT images.

Leaf ionome and shoot biomass analyses

The elemental profiles of the shoots were measured using Inductively Coupled Plasma Mass Spectrometry (ICP-MS). The shoot biomass from all uprooted plants was dried in an oven at 225˚C for 12 hours and then weighed. The dried biomass samples were cut into small pieces using a clean ceramic scalpel and placed in 5 ml Eppendorf tubes with 3 zirconium oxide beads. Shoots were pulverised using a Tissue Lyzer II (Qiagen) using 2 cycles of 60 seconds at the frequency of 30 s^{-1}. Next, 5-10 mg of pulverized shoot samples were weighted on a Mettler five-decimal analytical scale, and 1-3 mL (depending on the sample dry weight) of the concentrated trace metal grade nitric acid Primar Plus (Fisher Chemicals) was added to each tube. Prior to the digestion, 20 µg/L of Indium (In) was added to the nitric acid as an internal

standard to assess putative errors in dilution or variations in sample introduction and plasma stability in the ICP-MS instrument. The samples were then digested in DigiPREP MS dry block heaters (SCP Science; QMX Laboratories) for 4-h at 115˚C. After cooling down, the digests were diluted to 10-30 mL (depending on the volume of the nitric acid added) with 18.2 MΩcm Milli-Q Direct water. The elemental analysis was performed using an ICP-MS, PerkinElmer NexION 2000 equipped with Elemental Scientific Inc 4DXX FAST Dual Rinse autosampler, FAST valve and peristaltic pump. The instrument was fitted with a PFA-ST3 MicroFlow nebulizer, baffled cyclonic C3 high sensitivity glass spray chamber cooled to 2 ºC with PC3X Peltier heated/cooled inlet system, 2.0 mm i.d. quartz injector torch and a set of nickel cones. Twenty-four elements were monitored including the following stable isotopes: ^{7}Li, ^{11}B, ^{23}Na, ^{24}Mg, ^{31}P, ^{34}S, ^{39}K, ^{43}Ca, ^{48}Ti, ^{52}Cr, ^{55}Mn, ^{56}Fe, ^{59}Co, ^{60}Ni, ^{63}Cu, ^{66}Zn, ^{75}As, ^{82}Se, ^{85}Rb, ^{88}Sr, ^{98}Mo, ^{111}Cd, ^{208}Pb and ^{115}In. Helium was used as a collision gas in Kinetic Energy Discrimination mode (KED) at a flow rate of 4.5 mL/min while measuring Na, Mg, P, S, K, Ca, Ti, Cr, Mn, Fe, Ni, Cu, Zn, As, Se and Pb to exclude possible polyatomic interferences.

The remaining elements were measured in the standard mode. The instrument Syngistix™ software for ICP-MS v.2.3 (Perkin Elmer) automatically corrected any isobaric interferences. The ICP-MS measurements were performed in peak hopping scan mode with dwell times ranging from 25 to 50 ms depending on the element, 20 sweeps per reading and three replicates. The ICP-MS conditions were adjusted to an RF power of 1600 Watts and an auxiliary gas flow rate of 1.20 L/min. Torch alignment, nebuliser gas flow and quadrupole ion deflector (QID) voltages (in standard and KED mode) were optimized before analysis for highest intensities and lowest interferences (oxides and doubly charged ions levels lower than 2.5 %) with NexION Setup Solution containing 1 µg/L of Be, Ce, Fe, ln, Li, Mg, Pb and U in 1 % nitric acid using a standard built-in software procedure. To correct for variation between and within ICP-MS analysis runs, liquid reference material was prepared using pooled digested samples and run after the instrument calibration and then after every nine samples in all ICP-MS sample sets. Equipment calibration was performed at the beginning of each analytical run using seven multi-element calibration standards (containing 2 µg/L In internal standard) prepared by diluting 1000 mg/L single-element standards solutions (Inorganic Ventures; Essex Scientific Laboratory Supplies Ltd) with 10 % nitric acid. As a calibration blank, 10 % nitric acid containing 2 µg/L In internal standard was used, and it was run throughout the analysis. Sample concentrations were calculated using the external calibration method within the instrument software. Further data processing, including the calculation of final element concentrations, was performed in Microsoft Excel.

Crown root transcriptomics

RNA extraction and sequencing

For RNA extractions and sequencing, flash-frozen crown roots were freeze-dried for 48 hours and finely ground with pellet pestles. The RNA extraction protocol was carried out according to the NucleoSpin RNA Plant kit (Macherey-Nagel, Düren, Germany).

For the 132 maize samples, remnant DNA was removed from purified RNA using the DNA-Free kit (Invitrogen, Carlsbad, CA, USA). RNA-seq libraries were prepared using the QuantSeq 3' mRNA-Seq V2 kit with unique dual sequences and the unique molecular identifier (UMI) module (Lexogen, Vienna, Austria) following the manufacturer's recommendations. Libraries were pooled at equimolar concentrations and then sequenced (150bp) on a NovaSeq S4 flow cell (Illumina, San Diego, CA, USA) along with a 25% PhiX spike-in. Maize RNA-seq library preparations and sequencing were performed by the RTSF Genomics Core at Michigan State University.

For the 132 *T. dactyloides* samples, RNA-seq libraries were prepared using the NEBNext Ultra II Directional Library Kit with the oligo-dT magnetic isolation module (New England Biolabs, Ipswich, MA, USA) and sequenced on the Illumina NovaSeq 6000 platform at the Genomic Sciences Laboratory at North Carolina State University to generate a minimum of 40M read pairs (2x150bp) per sample.

Sequence processing

For the maize sequence reads, UMIs were removed from all sequences and added to the read headers using UMI-tools (Smith, Heger, and Sudbery 2017). Next, cutadapt version 4.2 (Martin 2011) was used to remove the first four bases of each read, remove poly-A tails (if present), remove spurious poly-G runs using the --nextseq-trim=10 parameter, and remove adapter sequences. Reads that were <10 bp long or that aligned to maize rRNA gene sequences were removed; the remaining reads were aligned to the maize reference genome B73 RefGen_v5 (Hufford et al. 2021) using HISAT2 version 2.2.1 (Kim et al. 2019). Aligned reads were converted to BAM format, sorted, and indexed using samtools version 1.9 (Li et al. 2009). We then used UMI-tools (Smith, Heger, and Sudbery 2017) to de-duplicate reads that both shared a UMI and had identical mapping coordinates. Finally, we used the FeatureCounts function of the subread package version 2.0.5 (Liao, Smyth, and Shi 2014) with the maize genome annotation version Zm00001eb.1 and parameters -O --fraction -M --primary -g ID -t gene to generate a table of gene expression estimates.

For the *T. dactyloides* sequence reads, we first used cutadapt to remove NEBNext adapter sequences, poly-A tails, spurious poly-G runs, and low-quality tails using the -q 20,20 parameter and other default parameters. The cleaned reads were aligned to the *T. dactyloides* reference genome (Td-KS_B6_1-REFERENCE-PanAnd-2.0a; should be (Li et al. 2009) using HISAT2. The alignments were name-sorted

so that mate-pairs could be fixed using the fixmate function of samtools (Danecek et al. 2021), and then re-sorted based on coordinates, de-duplicated, and converted to indexed BAM files using the same software. Finally, a table of transcript expression estimates was generated using the FeatureCounts function of the subread package with parameters -p -O --fraction -M --primary -g ID -t gene and the *T. dactyloides* genome annotation version Td-KS_B6_1-REFERENCE-PanAnd-2.0a_Td00002ba.2.

Statistical analyses

Because the maize and *T. dactyloides* RNA-seq datasets were generated using different approaches (3' tag sequencing *vs.* full-length sequencing, respectively) we analyzed them in parallel rather than comparing them directly. For each species, we used DESeq2 (Love, Huber, and Anders 2014) to identify genes that were differentially expressed between plants inoculated with microbiomes from a low-precipitation climate ("dry legacy") *vs.* those inoculated with microbiomes from a high-precipitation climate ("wet legacy"). A single negative binomial model with default parameters was used to estimate $\log_2$-fold changes in gene expression due to inoculum legacy, while also controlling for the other experimental factors, using the model:

$$\text{Counts} \sim \text{Legacy} + \text{ConditioningPhaseWater} + \text{ConditioningPhaseHost} + \text{TestPhaseWater}$$

Statistical support was obtained using the Wald test with Benjamini-Hochberg FDR correction. All available samples were included in each analysis; thus, these results should be interpreted as the gene expression response to microbiome precipitation legacy, averaged across all levels of the other experimental factors.

In addition, we investigated whether plants' gene expression responses to limited *vs.* ample water during the Test Phase were affected by inoculum precipitation legacy. To do so, we used DESeq2 to fit a model with the formula Counts ~TestPhaseWater*Legacy. Then, we extracted the estimated $\log_2$-fold changes due to acute drought (relative to well-watered conditions) for both dry-legacy-inoculated and wet-legacy-inoculated plants. We inferred a meaningful interaction between these variables when the 95% confidence intervals of the two drought-induced $\log_2$-fold changes did not overlap at all. These interacting genes are candidates for linking real-time plant drought response to the microbiome's historical environmental conditions.

Finally, we conducted a mediation analysis to determine whether the *T. dactyloides* genes that were sensitive to inoculum legacy were implicated in phenotypic responses to subsequent acute drought. A gene was considered legacy-sensitive if its expression was significantly affected by the main effect of inoculum legacy, or if it was affected by the interaction between inoculum legacy and test phase drought treatment,

as described above. We summarized expression patterns of this subset of genes (normalized as transcripts per million, calculated using the full set of expressed genes) using non-metric multidimensional scaling of the Bray-Curtis distances among all *T. dactyloides* plants, which resulted in two axes of variation: MDS1 and MDS2. Next, we used the mediation package in R (Yimer et al. 2023) to compare the direct effects of test phase drought treatment on each focal plant trait (see *Plant trait feature selection*) to the indirects of the drought treatment mediated through MDS1 and MDS2. Each mediation analysis used the linear models:

Trait value ~ MDS + Test phase drought treatment
MDS ~ Test phase drought treatment

where MDS represents the "site score" of each individual plant on either MDS1 or MDS2. Separate models were fit to test the potential roles of MDS1 and MDS2 as mediator variables; however, a follow-up analysis using both MDS1 and MDS2 as simultaneous mediators, implemented in lavaan (Rosseel 2012), yielded equivalent conclusions.

Gene annotation

We downloaded maize and eastern gamagrass genome assemblies and annotations from MaizeGDB (Hufford et al. 2021; Portwood et al. 2019). Functional information for maize genes was taken from the *Zea mays* genome annotation version Zm-B73-REFERENCE-NAM-5.0_Zm00001eb.1 and accessed using MaizeGDB's MaizeMine tool (Hufford et al. 2021; Portwood et al. 2019; Woodhouse et al. 2021; Shamimuzzaman et al. 2020). For *Tripsacum dactyloides* genes, we relied on DNA sequence homology with annotated maize genes to infer function. We used BEDtools (Quinlan 2014) to extract gene coordinates and protein-coding sequences from the *T. dactyloides* reference genome Td-KS_B6_1-REFERENCE-PanAnd-2.0a, and then used OrthoFinder (Emms and Kelly 2019) to compare coding sequences from the two species. OrthoFinder identified 32,785 *T. dactyloides* genes (71.5% of the total) as homologs of maize genes, grouping them into 21,658 distinct orthogroups. All differential gene expression analyses, however, considered the entire set of expressed genes; those without maize orthologs, or with unannotated maize orthologs, were considered to be of unknown function.

Amplicon sequencing: DNA extractions and library preps

One crown root from each plant was cut off with a ceramic blade and placed in a 1.7 mL tube and flash frozen in liquid nitrogen for downstream amplicon library preparation. After collection, root sub-samples were kept on dry ice and ceramic tweezers were used to transfer the whole root to 1.1 mL cluster tubes (USA Scientific, Ocala, FL, USA). Tweezers were sterilized with 80% EtOH between samples. Roots were selected at random for placement in cluster tubes and were stored at -80ºC until DNA extraction, at

which time roots were freeze-dried for 48 hours in a FreeZone lyophilizer (Labconco, Kansas City, MO, USA). After freeze-drying, roots were flash frozen in liquid nitrogen. To break apart thick roots, sterile forceps and a dissecting needle were used before placing the rack of cluster tubes in an HT Lysing Homogenizer (OHAUS, Parsippany, NJ, USA) with two clean 5/32" steel balls in each tube. Samples were homogenized at 25 Hz for 1 min. Root material was then transferred to 2 mL bead-beating 96-well plates containing sterile 1 mm garnet beads with 850 µL of lysis buffer (1M Tris, pH = 8.0; 100 mM NaCl; 10 mM EDTA). For each plate, a positive (ZymoBiomics Microbial Community Standard) and negative control, 800 µL of lysis buffer, were included. Bead-beating plates were stored at -20ºC until extraction. After thawing, 10 µL of 20% sodium dodecyl sulfate (SDS) was added to each well before homogenizing for a total of 20 min at 20 Hz. Plates were incubated in a water bath (55ºC for 90 min) and centrifuged (6 min at 4500 x g). 400 µL of the resulting supernatant was transferred to new 1 mL 96-well plates containing 120 µL of 5 M potassium acetate in each well and incubated overnight at -20ºC. After thawing the plates, they were centrifuged (6 min at 4500 x g) and 400 µL of the supernatant was transferred to a new 1 mL 96-well plate containing 600 µL of diluted SPRI-bead solution (protocol derived from that of Rohland & Reich, 2012). These plates were mixed thoroughly for 5 min at 1000 rpm on an orbital plate shaker. Samples were allowed to incubate for 10 min so DNA could bind to beads, after which the plate was centrifuged (6 min at 4500 x g) and placed on a magnet rack for 10 min. The supernatant was removed, and the beads were washed twice with 900 µL of 80% EtOH. After washing, the supernatant was decanted and the beads were air dried. DNA was eluted in 75 µL of pre-heated 1x TE (pH = 7.5; 37ºC) and transferred to clean 0.45 mL plates and stored at -20ºC.

16S-v4 amplification was performed on DNA extractions with paired 515f/806r primers (Parada, Needham, and Fuhrman 2016; Apprill et al. 2015). PCR reactions contained DreamTaq Master Mix (Thermo Fisher Scientific, Waltham, MA, USA), 10 mg/µL bovine serum albumin (BSA), 100 uM peptide nucleic acid (PNA), and PCR-grade water. BSA was used to enhance PCR amplification while PNA was used to suppress primer binding and subsequent amplification of mitochondrial and chloroplast 16S regions (Lundberg et al. 2013). The PCR included an initial denaturation step at 95ºC for 2 min, followed by 27 cycles of an additional denaturation at 95ºC for 20 s, PNA annealing at 78ºC for 5 s, primer annealing at 52ºC for 20 s, and extension at 72ºC for 50 s. This was followed by a final extension step for 10 min at 72ºC. PCR products were purified with the ExoSAP reagent. Briefly, a well-mixed combination of 0.78 µL of PCR-grade water, 0.02 µL of 10 U/µL exonuclease I (Applied Biosystems), and 0.2 µL of 1U/µL shrimp alkaline phosphatase (Applied Biosystems) was added to each 10 µL PCR product. The ExoSAP reagent and PCR products were vortexed and incubated at 37ºC for 20 min, followed by 15 min at 80ºC. Two µL of the purified amplicons were used as template DNA in an indexing PCR to attach barcoded P5 and P7 Illumina adaptors. The 10 µL reaction included 5 µM each of P5 and P7 adaptors, 1x DreamTaq Master

Mix (Thermo Fisher Scientific), 10 mg/mL BSA, 100 µM PNA, and PCR-grade water. An initial denaturation step was performed at 95ºC for 2 min. For 8 cycles, an additional denaturation was carried out at 95ºC for 20 s, PNA annealing at 78ºC for 5 s, primer annealing at 52ºC for 20 s, and extension at 72ºC for 50 s. A final extension step was performed at 72ºC for 10 min. PCR products were verified via 2% agarose gel electrophoresis and then pooled by 96-well plate using the "Just-a-Plate" PCR cleanup and normalization kit (Charm Biotech, St. Louis, MO, USA). Pools were size selected and combined in equimolar concentrations before being sequenced on an Illumina SP flow cell on the NovaSeq 6000 platform (2x250bp reads).

Test phase amplicon data and plant trait data analyses

We removed primer sequences from raw 16S-v4 Illumina reads using cutadapt (Martin 2011), requiring at least 5 nucleotides of overlap. Additional quality control and processing was performed with the DADA2 software (Callahan et al. 2016). Forward reads were discarded if they had more than 6 expected errors, otherwise they were truncated at 200 nucleotides; for reverse reads the parameters were 7 expected errors and 170 nucleotides. Error rates were estimated separately for forward and reverse reads based on a sample of 1x108 bases, then used to denoise and dereplicate reads using the standard DADA2 functions. Chimeric sequences were detected and removed using the "consensus" procedure in DADA2. Each individual sample was processed in parallel, after which all of the resulting amplicon sequence variant (ASV) tables were merged. Finally, taxonomy of each ASV was assigned by comparison to the RDP database (Cole et al. 2014).

Root microbiome diversity analyses.

All statistical analyses were performed using R (v4.4.0). The cleaned and prepared microbiome data, as phyloseq objects, were loaded into R. The phyloseq object sample data table was replaced with an updated metadata file. The "mock" samples were removed from the dataset and the data was subset by the test phase host, maize and gamagrass using phyloseq::subset_samples (v1.48.0). Maize and gamagrass root bacterial microbiome Shannon Diversity was fit to a mixed-effects model using the lme4 (v1.1-35.4) package and lmer() function, using the following model:

expShannon~TestWater+Legacy + (1|DNAplate)

A type III ANOVA was performed using stats::anova() to test for significance, followed by pairwise comparisons and significance tests using emmeans (v1.10.2) package with false discovery rate adjustments. Data visualizations were generated using ggplot2 (v3.5.1), the error bars represent standard

error and the points are estimated marginal means. All plots were saved in PDF format. Composite figures were created in Adobe Illustrator.

Bacterial community beta diversity was accessed with a Constrained Analysis of Principal Coordinates, using phyloseq::ordinate, method="CAP", and distance="euclidean of the following formulas:

~Legacy+Condition(DNAplate)+Condition(CondHost)+Condition(CondWater)+Condition(TestWater)

~TestWater+Condition(DNAplate)+Condition(CondHost)+Condition(CondWater)+Condition(Legacy)

An ANOVA-like permutation test was used to test for model significance using the vegan::anova.cca() function. CAP1 and MDS1 axes were plotted using ggplot2, including 95% confidence interval ellipse (stat_ellipse()) . To evaluate treatment group beta-dispersion, euclidean distances were calculated for the center-log ration transformed counts using phyloseq::distance(). Both "Legacy" and "TestWater" terms were tested for beta-dispersion differences using the euclidean distances matrix and vegan::betadisper() and vegan::permutest() to test for significance. Distances were then extracted from the results output and fit to a linear model. Estimated marginal means were calculated and plotted using the same methods as above. The error bars represent standard error.

Then, an ASV differential abundance analysis was performed of gamagrass and maize associated ASVs separately. Center-log ratio transformed counts of ASVs each fit to a linear model using an iterative for loop. Each ASV was subset using phyloseq:subset_taxa and the phyloseq::psmelt() function was used to reformat the phyloseq object into a dataframe. Then the ASV abundance was fit to the following model:

Abundance ~ Legacy*TestWater

Then, stats::anova() was used to test for significance, followed by an FDR p adjustment using p.adjust(). ASVs with significant (≤0.05) adjusted p-values for the Legacy*TestWater interaction terms were extracted and z-scores of the center-log ration transformed counts were plotted in a heatmap using pheatmap::pheatmap() with clustering_method="complete".

Plant trait feature selection.

All plant data was loaded into Rstudio. The intrinsic water use efficiency (iWUE) was calculated using the ratio of photosynthetic rate (A) and stomatal conductance (gs) or A/gs ((μmol m^{-2} s^{-1})/(mol m^{-2} s^{-1})). Data was subset by Test phase host treatment groups (gamagrass and maize). For the feature selection, the "mock" treatment was removed. The 67 features that were selected for testing were subset into a dataframe. Three sample rows were removed from the dataset because they had missing data. Drought susceptibility index (S-index) was calculated for each of these features using the following formula:

$$S=Trait_{drought}/mean(Trait_{control})$$

Then, for each host, a random forest model was used to select the top 10 most important features from the 67 total s-index measurements using randomForest(), with "Legacy" as the predictor. Correlations were estimated for the top ten traits and if any two of the top 10 traits were highly correlated ($r \geq 0.7$), the trait that ranked lower in the random forest model was removed (Extended Data Fig 7). Non-correlative top features from the test water treatment groups (drought vs. watered control) were combined for each test phase host (maize and gamagrass). Vegan:rda() was used to perform a redundancy analysis on the top features using the following formula:

Top_features~ Legacy + Condition(CondGroup), scale=TRUE

An ANOVA-like permutation test was used to test for model significance using the vegan::anova.cca() function. A biplot was created using ggplot2 plotting RDA1 and PC1 axes, as well as the species scores (represented by arrows), and stat_ellipse was used to plot 95% confidence intervals of the site scores.

Finally, s-indices for each of the top features and iWUE were fit to mixed effects models, when possible, or a linear model if overfitting of the mixed effects model occurred. Each feature or trait was visually assessed for outliers, which were removed. Removing the outliers did not impact the interpretation of any of the results. Formulas using for the mixed effects or linear model, respectively, include:

lmer(s-index ~ Legacy + (1|CondGroup))

lm(s-index ~ Legacy + CondGroup)

The fit of the model was accessed and if needed, the s-index was transformed using sqrt(), exp(), or log() to improve the fit. ANOVA was used to assess significance and estimated marginal means were calculated and plotted as described above.

ACKNOWLEDGMENTS

We thank Arun Seetharam, Matthew Hufford, and the PanAnd consortium for granting early access to the *Tripsacum dactyloides* genome and annotation. We thank Dr. Mitch Greer, Michaela VonLintel, Justin Roemer, Dr. Alan Schlegel, and the Nature Conservancy for granting access to soil collection sites in Kansas, and Dr. Peter Balint-Kurti for providing maize seeds. We are grateful to the undergraduate student researchers and technicians who helped to set up experiments and collect data: Felicity Tso, Hannah Reid, and Carmen Rodriguez. This work was supported by a UKRI/BBSRC - NSF/BIO Lead Agency Opportunity, National Science Foundation award #IOS-2016351 and BBSRC grant #BB/V011294/1. Maize root transcriptome library preps and sequencing were performed in the RTSF Genomics Core at Michigan State University. *T. dactyloides* library preps and RNA-seq were performed at the NC State University Genomic Sciences Laboratory (Raleigh, NC, USA). Research reported in this publication was made possible in part by the services of the KU Genome Sequencing Core. This lab is supported by the National Institute of General Medical Sciences (NIGMS) of the National Institutes of Health under award number P30GM145499. We thank the University of Kansas Medical Center – Genomics Core for generating the 16S amplicon sequence data sets. The Genomics Core is supported by the Kansas Intellectual and Developmental Disabilities Research Center (NIH U54 HD 090216), the Molecular Regulation of Cell Development and Differentiation – COBRE (P30 GM122731), The NIH S10 High End Instrumentation Grant (NIH S10OD021743) and the Frontiers CTSA Grant (UL1TR002366).

REFERENCES

Ahmed, Mutez Ali, Mohsen Zarebanadkouki, Félicien Meunier, Mathieu Javaux, Anders Kaestner, and Andrea Carminati. 2018. "Root Type Matters: Measurement of Water Uptake by Seminal, Crown, and Lateral Roots in Maize." *Journal of Experimental Botany* 69 (5): 1199–1206.

Apprill, A., S. McNally, R. Parsons, and L. Weber. 2015. "Minor Revision to V4 Region SSU rRNA 806R Gene Primer Greatly Increases Detection of SAR11 Bacterioplankton." *Aquatic Microbial Ecology: International Journal* 75 (2): 129–37.

Batstone, Rebecca T., Anna M. O'Brien, Tia L. Harrison, and Megan E. Frederickson. 2020. "Experimental Evolution Makes Microbes More Cooperative with Their Local Host Genotype." *Science* 370 (6515): 476–78.

"BBTools." 2016. DOE Joint Genome Institute. September 1, 2016. https://jgi.doe.gov/data-and-tools/bbtools/.

Beven, K., and P. Germann. n.d. "Macropores and Water Flow in Soils." *Water Resources Research*. https://doi.org/10.1029/WR018i005p01311.

Breitwieser, Florian P., and Steven L. Salzberg. 2020. "Pavian: Interactive Analysis of Metagenomics Data for Microbiome Studies and Pathogen Identification." *Bioinformatics* 36 (4): 1303–4.

Buchfink, Benjamin, Klaus Reuter, and Hajk-Georg Drost. 2021. "Sensitive Protein Alignments at Tree-of-Life Scale Using DIAMOND." *Nature Methods* 18 (4): 366–68.

Callahan, Benjamin J., Paul J. McMurdie, Michael J. Rosen, Andrew W. Han, Amy Jo A. Johnson, and

Susan P. Holmes. 2016. "DADA2: High-Resolution Sample Inference from Illumina Amplicon Data." *Nature Methods* 13 (7): 581–83.
Canarini, Alberto, Hannes Schmidt, Lucia Fuchslueger, Victoria Martin, Craig W. Herbold, David Zezula, Philipp Gündler, et al. 2021. "Ecological Memory of Recurrent Drought Modifies Soil Processes via Changes in Soil Microbial Community." *Nature Communications* 12 (1): 5308.
Cantalapiedra, Carlos P., Ana Hernández-Plaza, Ivica Letunic, Peer Bork, and Jaime Huerta-Cepas. 2021. "eggNOG-Mapper v2: Functional Annotation, Orthology Assignments, and Domain Prediction at the Metagenomic Scale." *Molecular Biology and Evolution* 38 (12): 5825–29.
Chase, Alexander B., Claudia Weihe, and Jennifer B. H. Martiny. 2021. "Adaptive Differentiation and Rapid Evolution of a Soil Bacterium along a Climate Gradient." *Proceedings of the National Academy of Sciences of the United States of America* 118 (18). https://doi.org/10.1073/pnas.2101254118.
Chaumont, F., F. Barrieu, E. Wojcik, M. J. Chrispeels, and R. Jung. 2001. "Aquaporins Constitute a Large and Highly Divergent Protein Family in Maize." *Plant Physiology* 125 (3): 1206–15.
Cole, James R., Qiong Wang, Jordan A. Fish, Benli Chai, Donna M. McGarrell, Yanni Sun, C. Titus Brown, Andrea Porras-Alfaro, Cheryl R. Kuske, and James M. Tiedje. 2014. "Ribosomal Database Project: Data and Tools for High Throughput rRNA Analysis." *Nucleic Acids Research* 42 (Database issue): D633–42.
Custódio, Valéria, Mathieu Gonin, Georg Stabl, Niokhor Bakhoum, Maria Margarida Oliveira, Caroline Gutjahr, and Gabriel Castrillo. 2022. "Sculpting the Soil Microbiota." *The Plant Journal: For Cell and Molecular Biology* 109 (3): 508–22.
Danecek, Petr, James K. Bonfield, Jennifer Liddle, John Marshall, Valeriu Ohan, Martin O. Pollard, Andrew Whitwham, et al. 2021. "Twelve Years of SAMtools and BCFtools." *GigaScience* 10 (2). https://doi.org/10.1093/gigascience/giab008.
De Coster, Wouter, Svenn D'Hert, Darrin T. Schultz, Marc Cruts, and Christine Van Broeckhoven. 2018. "NanoPack: Visualizing and Processing Long-Read Sequencing Data." *Bioinformatics* 34 (15): 2666–69.
Dexter, A. R. 2004. "Soil Physical Quality: Part I. Theory, Effects of Soil Texture, Density, and Organic Matter, and Effects on Root Growth." *Geoderma* 120 (3): 201–14.
Dixon, Groves B., Sarah W. Davies, Galina V. Aglyamova, Eli Meyer, Line K. Bay, and Mikhail V. Matz. 2015. "Genomic Determinants of Coral Heat Tolerance across Latitudes." *Science* 348 (6242): 1460–62.
Emms, David M., and Steven Kelly. 2019. "OrthoFinder: Phylogenetic Orthology Inference for Comparative Genomics." *Genome Biology* 20 (1): 238.
Evans, Sarah, Steven Allison, and Christine Hawkes. 2022. "Microbes, Memory and Moisture: Predicting Microbial Moisture Responses and Their Impact on Carbon Cycling." *Functional Ecology*, March. https://doi.org/10.1111/1365-2435.14034.
Gao, Yingzhi, and Jonathan P. Lynch. 2016. "Reduced Crown Root Number Improves Water Acquisition under Water Deficit Stress in Maize (Zea Mays L.)." *Journal of Experimental Botany* 67 (15): 4545–57.
Gil-Quintana, Erena, Estíbaliz Larrainzar, Amaia Seminario, Juan Luis Díaz-Leal, Josefa M. Alamillo, Manuel Pineda, Cesar Arrese-Igor, Stefanie Wienkoop, and Esther M. González. 2013. "Local Inhibition of Nitrogen Fixation and Nodule Metabolism in Drought-Stressed Soybean." *Journal of Experimental Botany* 64 (8): 2171–82.
Grabherr, Manfred G., Brian J. Haas, Moran Yassour, Joshua Z. Levin, Dawn A. Thompson, Ido Amit, Xian Adiconis, et al. 2011. "Full-Length Transcriptome Assembly from RNA-Seq Data without a Reference Genome." *Nature Biotechnology* 29 (7): 644–52.
Huerta-Cepas, Jaime, Damian Szklarczyk, Davide Heller, Ana Hernández-Plaza, Sofia K. Forslund, Helen Cook, Daniel R. Mende, et al. 2019. "eggNOG 5.0: A Hierarchical, Functionally and Phylogenetically Annotated Orthology Resource Based on 5090 Organisms and 2502 Viruses." *Nucleic Acids Research* 47 (D1): D309–14.

Hufford, Matthew B., Arun S. Seetharam, Margaret R. Woodhouse, Kapeel M. Chougule, Shujun Ou, Jianing Liu, William A. Ricci, et al. 2021. "De Novo Assembly, Annotation, and Comparative Analysis of 26 Diverse Maize Genomes." *Science* 373 (6555): 655–62.

Hund, Andreas, Nathinee Ruta, and Markus Liedgens. 2009. "Rooting Depth and Water Use Efficiency of Tropical Maize Inbred Lines, Differing in Drought Tolerance." *Plant and Soil* 318 (1-2): 311–25.

Kim, Daehwan, Joseph M. Paggi, Chanhee Park, Christopher Bennett, and Steven L. Salzberg. 2019. "Graph-Based Genome Alignment and Genotyping with HISAT2 and HISAT-Genotype." *Nature Biotechnology* 37 (8): 907–15.

Klein, Stephanie P., Hannah M. Schneider, Alden C. Perkins, Kathleen M. Brown, and Jonathan P. Lynch. 2020. "Multiple Integrated Root Phenotypes Are Associated with Improved Drought Tolerance." *Plant Physiology* 183 (3): 1011–25.

Kolmogorov, Mikhail, Derek M. Bickhart, Bahar Behsaz, Alexey Gurevich, Mikhail Rayko, Sung Bong Shin, Kristen Kuhn, et al. 2020. "metaFlye: Scalable Long-Read Metagenome Assembly Using Repeat Graphs." *Nature Methods* 17 (11): 1103–10.

Kopylova, Evguenia, Laurent Noé, and Hélène Touzet. 2012. "SortMeRNA: Fast and Accurate Filtering of Ribosomal RNAs in Metatranscriptomic Data." *Bioinformatics* 28 (24): 3211–17.

Lebeis, Sarah L., Sur Herrera Paredes, Derek S. Lundberg, Natalie Breakfield, Jase Gehring, Meredith McDonald, Stephanie Malfatti, et al. 2015. "PLANT MICROBIOME. Salicylic Acid Modulates Colonization of the Root Microbiome by Specific Bacterial Taxa." *Science* 349 (6250): 860–64.

Lee, Dong-Keun, Pil Joong Chung, Jin Seo Jeong, Geupil Jang, Seung Woon Bang, Harin Jung, Youn Shic Kim, Sun-Hwa Ha, Yang Do Choi, and Ju-Kon Kim. 2017. "The Rice OsNAC6 Transcription Factor Orchestrates Multiple Molecular Mechanisms Involving Root Structural Adaptions and Nicotianamine Biosynthesis for Drought Tolerance." *Plant Biotechnology Journal* 15 (6): 754–64.

Liao, Yang, Gordon K. Smyth, and Wei Shi. 2014. "featureCounts: An Efficient General Purpose Program for Assigning Sequence Reads to Genomic Features." *Bioinformatics* 30 (7): 923–30.

Li, Heng. 2018. "Minimap2: Pairwise Alignment for Nucleotide Sequences." *Bioinformatics* 34 (18): 3094–3100.

Li, Heng, Bob Handsaker, Alec Wysoker, Tim Fennell, Jue Ruan, Nils Homer, Gabor Marth, Goncalo Abecasis, Richard Durbin, and 1000 Genome Project Data Processing Subgroup. 2009. "The Sequence Alignment/Map Format and SAMtools." *Bioinformatics* 25 (16): 2078–79.

Love, Michael I., Wolfgang Huber, and Simon Anders. 2014. "Moderated Estimation of Fold Change and Dispersion for RNA-Seq Data with DESeq2." *Genome Biology* 15 (12): 550.

Lu, Jennifer, Florian P. Breitwieser, Peter Thielen, and Steven L. Salzberg. 2017. "Bracken: Estimating Species Abundance in Metagenomics Data." *PeerJ. Computer Science* 3 (e104): e104.

Lundberg, Derek S., Scott Yourstone, Piotr Mieczkowski, Corbin D. Jones, and Jeffery L. Dangl. 2013. "Practical Innovations for High-Throughput Amplicon Sequencing." *Nature Methods* 10 (10): 999–1002.

Martin, Marcel. 2011. "Cutadapt Removes Adapter Sequences from High-Throughput Sequencing Reads." *EMBnet.journal* 17 (1): 10–12.

McMurdie, Paul J., and Susan Holmes. 2013. "Phyloseq: An R Package for Reproducible Interactive Analysis and Graphics of Microbiome Census Data." *PloS One* 8 (4): e61217.

Meijenfeldt, F. A. Bastiaan von, Ksenia Arkhipova, Diego D. Cambuy, Felipe H. Coutinho, and Bas E. Dutilh. 2019. "Robust Taxonomic Classification of Uncharted Microbial Sequences and Bins with CAT and BAT." *Genome Biology* 20 (1): 217.

Mendiburu, F. 2019. "Agricolae: Statistical Procedures for Agricultural Research." *(No Title)*. https://cir.nii.ac.jp/crid/1373101970110268292.

Morella, Norma M., Francis Cheng-Hsuan Weng, Pierre M. Joubert, C. Jessica E. Metcalf, Steven Lindow, and Britt Koskella. 2020. "Successive Passaging of a Plant-Associated Microbiome Reveals Robust Habitat and Host Genotype-Dependent Selection." *Proceedings of the National Academy of Sciences* 117 (2): 1148–59.

Naylor, Dan, Stephanie DeGraaf, Elizabeth Purdom, and Devin Coleman-Derr. 2017. "Drought and Host

Selection Influence Bacterial Community Dynamics in the Grass Root Microbiome." *The ISME Journal* 11 (12): 2691–2704.
Oksanen, J., F. Blanchet, R. Kindt, P. Legendre, R. G. O'Hara, G. L. Simpson, P. Minchin, and R. B. O'Hara. 2007. "Vegan : Community Ecology Package. R Package Version 1.8-5." https://mirror.ibcp.fr/pub/CRAN/web/packages/vegan/vegan.pdf.
Parada, Alma E., David M. Needham, and Jed A. Fuhrman. 2016. "Every Base Matters: Assessing Small Subunit rRNA Primers for Marine Microbiomes with Mock Communities, Time Series and Global Field Samples." *Environmental Microbiology* 18 (5): 1403–14.
Patro, Rob, Geet Duggal, Michael I. Love, Rafael A. Irizarry, and Carl Kingsford. 2017. "Salmon Provides Fast and Bias-Aware Quantification of Transcript Expression." *Nature Methods* 14 (4): 417–19.
Portwood, John L., 2nd, Margaret R. Woodhouse, Ethalinda K. Cannon, Jack M. Gardiner, Lisa C. Harper, Mary L. Schaeffer, Jesse R. Walsh, et al. 2019. "MaizeGDB 2018: The Maize Multi-Genome Genetics and Genomics Database." *Nucleic Acids Research* 47 (D1): D1146–54.
Quinlan, Aaron R. 2014. "BEDTools: The Swiss-Army Tool for Genome Feature Analysis." *Current Protocols in Bioinformatics / Editoral Board, Andreas D. Baxevanis ... [et Al.]* 47 (September):11.12.1–34.
Rosseel, Yves. 2012. "Lavaan: An R Package for Structural Equation Modeling." *Journal of Statistical Software* 48 (May):1–36.
Rousseva, S., D. Torri, and M. Pagliai. 2002. "Effect of Rain on the Macroporosity at the Soil Surface." *European Journal of Soil Science* 53 (1): 83–93.
Salas-González, Isai, Guilhem Reyt, Paulina Flis, Valéria Custódio, David Gopaulchan, Niokhor Bakhoum, Tristan P. Dew, et al. 2021. "Coordination between Microbiota and Root Endodermis Supports Plant Mineral Nutrient Homeostasis." *Science* 371 (6525). https://doi.org/10.1126/science.abd0695.
Sanchez-Moreno, Juan Francisco, Chris M. Mannaerts, and Victor Jetten. 2014. "Rainfall Erosivity Mapping for Santiago Island, Cape Verde." *Geoderma* 217-218 (April):74–82.
Schimel, Joshua, Teri C. Balser, and Matthew Wallenstein. 2007. "Microbial Stress-Response Physiology and Its Implications for Ecosystem Function." *Ecology* 88 (6): 1386–94.
Schulz, Philipp, Katrin Piepenburg, Ruth Lintermann, Marco Herde, Mark A. Schöttler, Lena K. Schmidt, Stephanie Ruf, Jörg Kudla, Tina Romeis, and Ralph Bock. 2021. "Improving Plant Drought Tolerance and Growth under Water Limitation through Combinatorial Engineering of Signalling Networks." *Plant Biotechnology Journal* 19 (1): 74–86.
Seethepalli, Anand, Kundan Dhakal, Marcus Griffiths, Haichao Guo, Gregoire T. Freschet, and Larry M. York. 2021. "RhizoVision Explorer: Open-Source Software for Root Image Analysis and Measurement Standardization." *AoB Plants* 13 (6): lab056.
Shamimuzzaman, Md, Jack M. Gardiner, Amy T. Walsh, Deborah A. Triant, Justin J. Le Tourneau, Aditi Tayal, Deepak R. Unni, et al. 2020. "MaizeMine: A Data Mining Warehouse for the Maize Genetics and Genomics Database." *Frontiers in Plant Science* 11 (October):592730.
Shetty, S. 2023. "Lahti L. Microbiomeutilities: Microbiomeutilities: Utilities for Microbiome Analytics. 2022."
Smith, Tom, Andreas Heger, and Ian Sudbery. 2017. "UMI-Tools: Modeling Sequencing Errors in Unique Molecular Identifiers to Improve Quantification Accuracy." *Genome Research* 27 (3): 491–99.
Soltanpour, P. N., and A. P. Schwab. 1977. "A New Soil Test for Simultaneous Extraction of Macro- and Micro-nutrients in Alkaline Soils." *Communications in Soil Science and Plant Analysis* 8 (3): 195–207.
Steinegger, Martin, and Johannes Söding. 2017. "MMseqs2 Enables Sensitive Protein Sequence Searching for the Analysis of Massive Data Sets." *Nature Biotechnology* 35 (11): 1026–28.
Sun, Yvonne, Brian J. Wilkinson, Theodore J. Standiford, Henry T. Akinbi, and Mary X. D. O'Riordan. 2012. "Fatty Acids Regulate Stress Resistance and Virulence Factor Production for Listeria

Monocytogenes." *Journal of Bacteriology* 194 (19): 5274–84.
Swift, Joel F., Matthew R. Kolp, Amanda Carmichael, Natalie E. Ford, Paige M. Hansen, Benjamin A. Sikes, Manuel Kleiner, and Maggie R. Wagner. 2024. "Drought Stress Homogenizes Maize Growth Responses to Diverse Natural Soil Microbiomes." *Plant and Soil*, July. https://doi.org/10.1007/s11104-024-06853-x.
Van der Jeugt, Felix, Peter Dawyndt, and Bart Mesuere. 2022. "FragGeneScanRs: Faster Gene Prediction for Short Reads." *BMC Bioinformatics* 23 (1): 198.
Vries, Franciska de, Jennifer Lau, Christine Hawkes, and Marina Semchenko. 2023. "Plant–soil Feedback under Drought: Does History Shape the Future?" *Trends in Ecology & Evolution* 38 (8): 708–18.
Woodcock, Stuart D., Karl Syson, Richard H. Little, Danny Ward, Despoina Sifouna, James K. M. Brown, Stephen Bornemann, and Jacob G. Malone. 2021. "Trehalose and α-Glucan Mediate Distinct Abiotic Stress Responses in Pseudomonas Aeruginosa." *PLoS Genetics* 17 (4): e1009524.
Wood, Derrick E., Jennifer Lu, and Ben Langmead. 2019. "Improved Metagenomic Analysis with Kraken 2." *Genome Biology* 20 (1): 257.
Woodhouse, Margaret R., Ethalinda K. Cannon, John L. Portwood 2nd, Lisa C. Harper, Jack M. Gardiner, Mary L. Schaeffer, and Carson M. Andorf. 2021. "A Pan-Genomic Approach to Genome Databases Using Maize as a Model System." *BMC Plant Biology* 21 (1): 385.
Wright, Rachel M., Galina V. Aglyamova, Eli Meyer, and Mikhail V. Matz. 2015. "Gene Expression Associated with White Syndromes in a Reef Building Coral, Acropora Hyacinthus." *BMC Genomics* 16 (1): 371.
Yimer, Belay B., Mark Lunt, Marcus Beasley, Gary J. Macfarlane, and John McBeth. 2023. "BayesGmed: An R-Package for Bayesian Causal Mediation Analysis." *PloS One* 18 (6): e0287037.
Zhang, Taiping, William S. Chandler, James M. Hoell, David Westberg, Charles H. Whitlock, and Paul W. Stackhouse. 2008. "A Global Perspective on Renewable Energy Resources: Nasa's Prediction of Worldwide Energy Resources (Power) Project." *Proceedings of ISES World Congress 2007 (Vol. I – Vol. V)*, 2636–40.
Zhou, Mei-Liang, Lei-Peng Qi, Jun-Feng Pang, Qian Zhang, Zhi Lei, Yi-Xiong Tang, Xue-Mei Zhu, Ji-Rong Shao, and Yan-Min Wu. 2013. "Nicotianamine Synthase Gene Family as Central Components in Heavy Metal and Phytohormone Response in Maize." *Functional & Integrative Genomics* 13 (2): 229–39.

EXTENDED DATA FIGURES

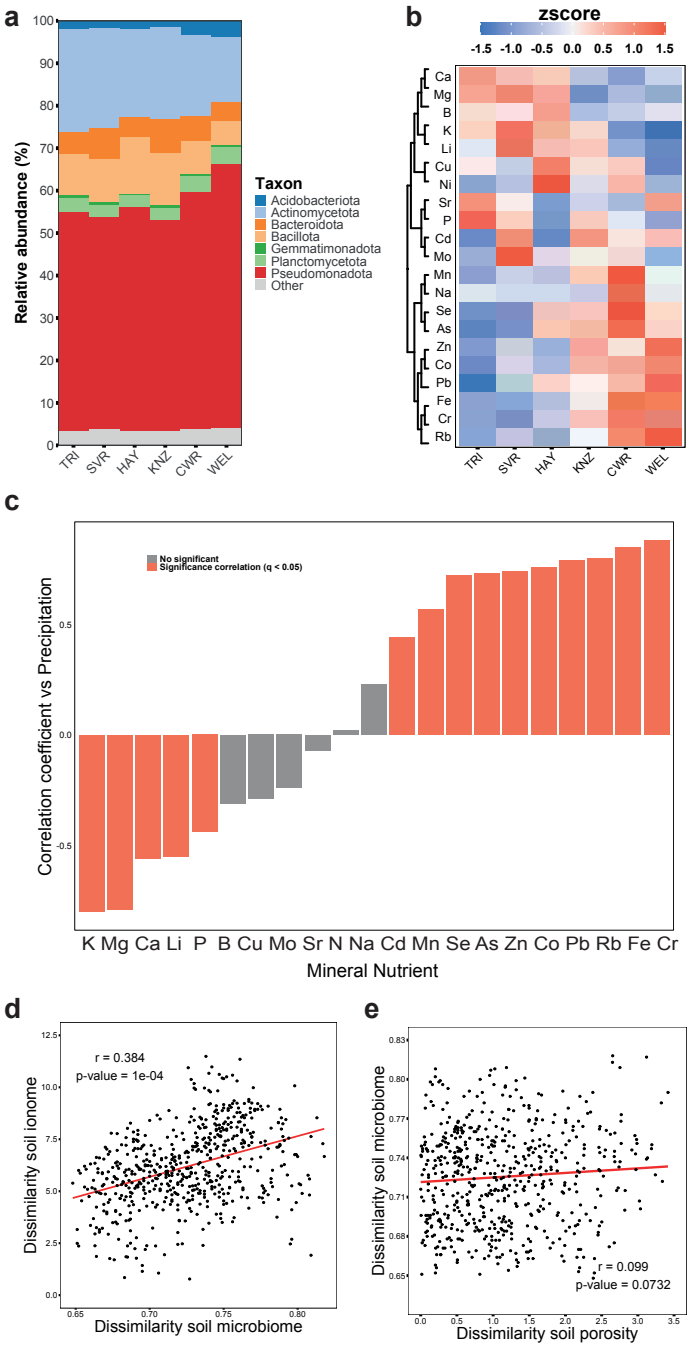

Extended Data Figure 1. Kansas soil properties varied across sites, including relative abundance shifts at the phyla-level (a), mineral nutrient concentrations across sites (b) and in association with the precipitation gradient (c). A Mantel test was used to test for associations between soil microbiome dissimilarities and soil mineral nutrient dissimilarities (d), and soil porosity dissimilarities (e).

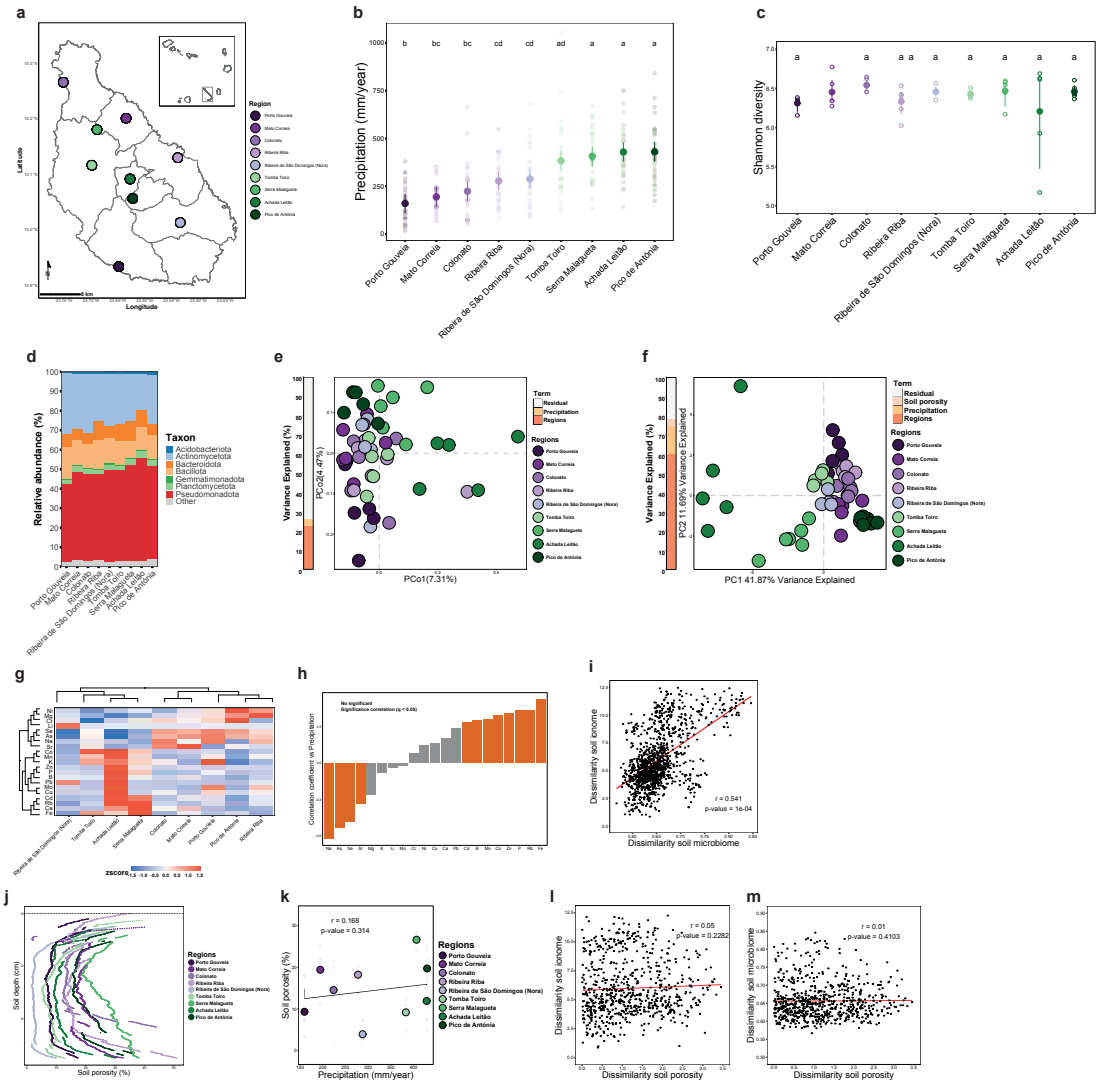

Extended Data Figure 2. Cabo Verde soil properties. a) A map of soil sample sites across Santiago Island, ranging in mean annual precipitation (b). c) Soil microbiome alpha diversity was similar across sites, but at the phyla-level the relative abundance of taxa differed in the dryer sites compared to the higher precipitation site (d). e) Soil site had a small, but significant impact on bacterial microbiome beta-diversity, but did not significantly impact mineral nutrient profile beta-diversity (f). Mineral nutrient concentrations varied across sample sites (g) and several significantly correlated with the precipitation gradient (h). i) Microbiome dissimilarities significantly correlated with mineral nutrient dissimilarities. j-k) Soil porosity was similar across all sample sites and did not significantly correlate with mineral nutrient dissimilarities (l) or microbiome dissimilarities (m).

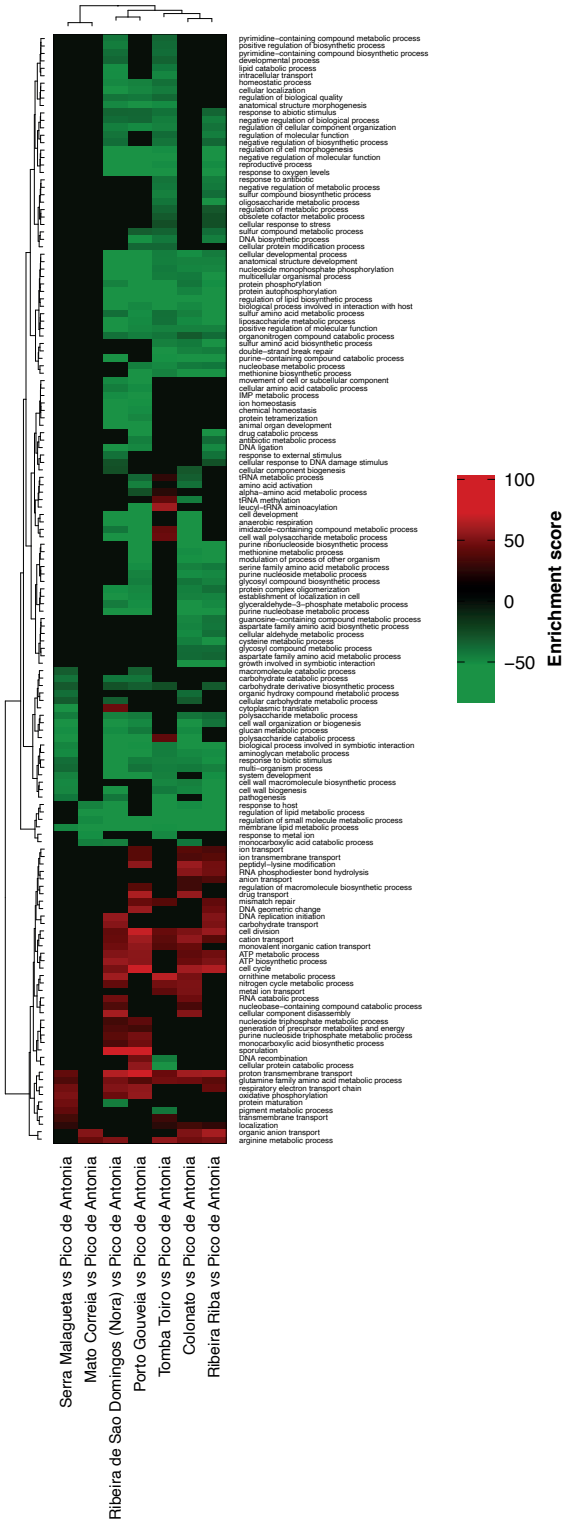

Extended Data Figure 3. Cabo Verde GO categories are differential abundance across soil samples. Red indicates GO categories were enriched in low precipitation soils and green indicates GO categories were depleted in low precipitation soils.

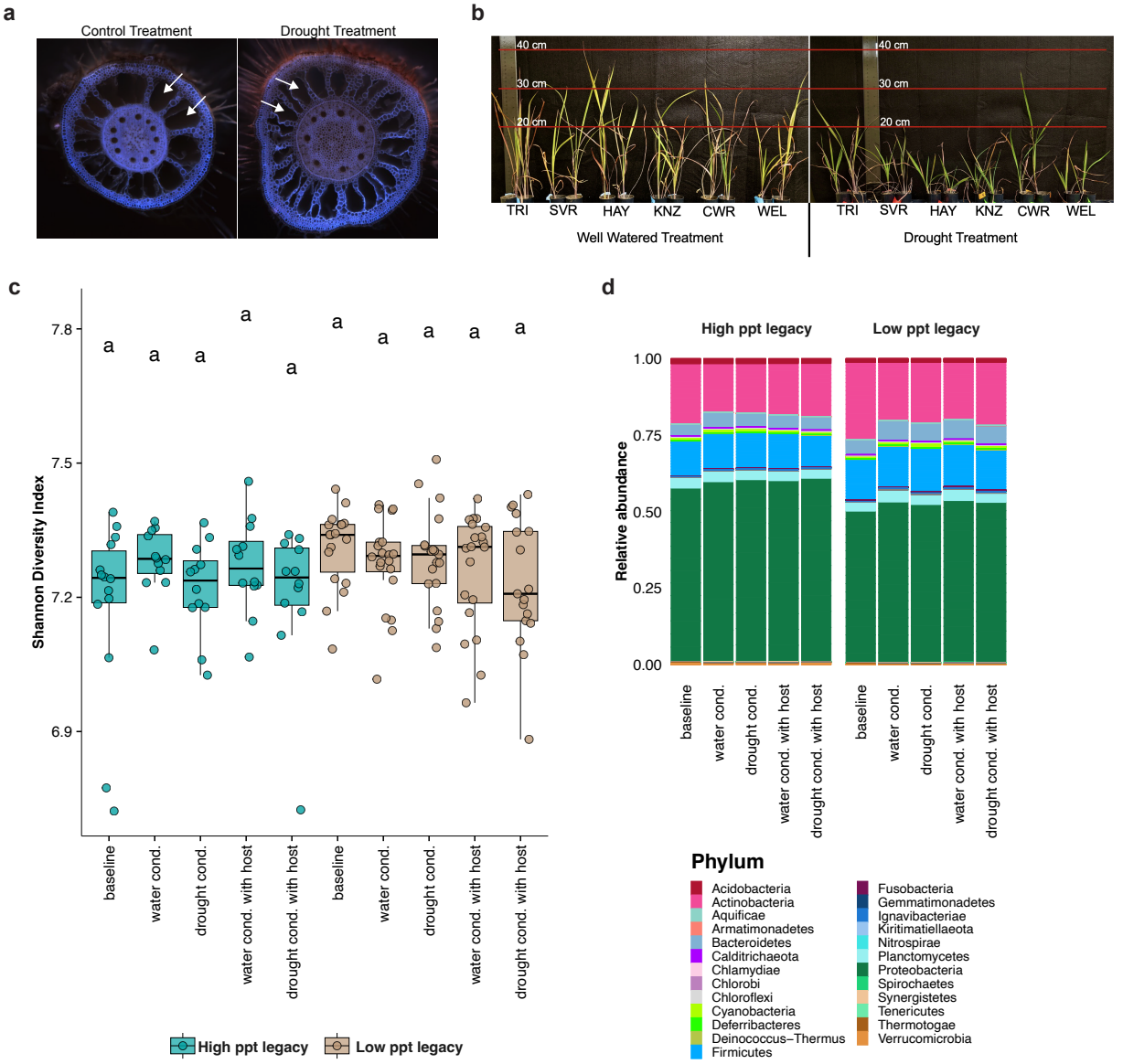

Extended Data Figure 4. Conditioning treatment effects on gamagrass and soil microbiome. a) Condition water treatment significantly impacted the number of root aerenchyma (a), determined using laser ablation topology imaging, and gamagrass shoot height (b). However, soil or rhizosphere bacterial community alpha diversity (c) and phyla-level relative abundance composition (d) was similar across all treatment groups.

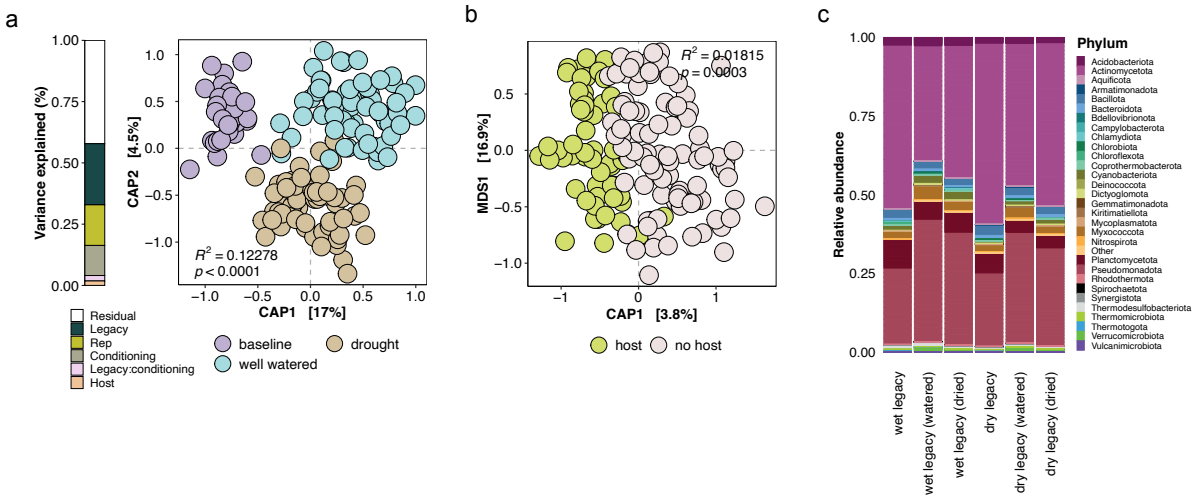

Extended Data Figure 5. Precipitation legacy metatranscriptome signatures are robust to perturbation. Compared to precipitation legacy, conditioning phase water (a) and host (b) treatments had lower, but significant impacts on the bacterial community transcriptional composition. c) Legacy effects impact the relative abundance of transcriptionally active bacteria at the phyla-level.

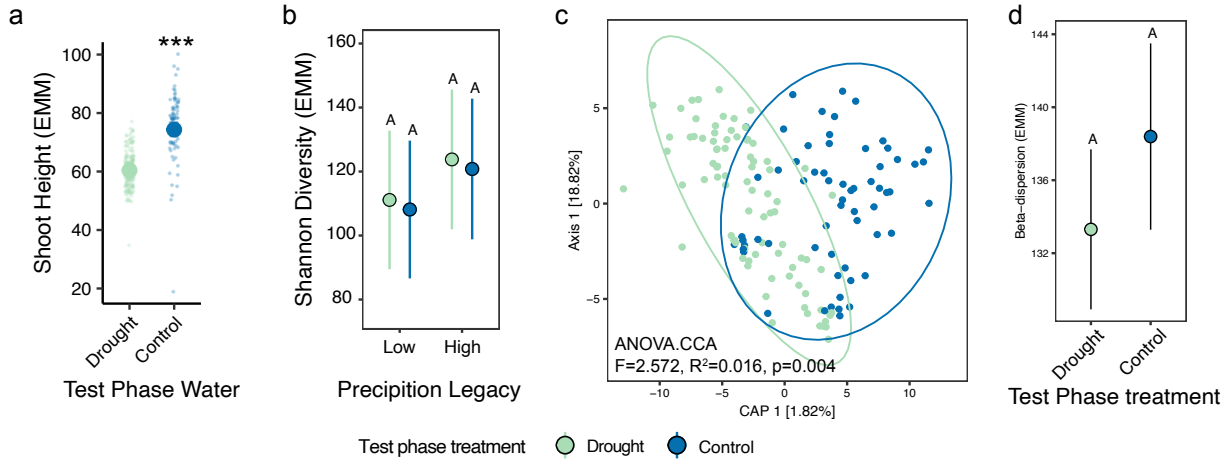

Extended Data Figure 6. Test phase gamagrass root microbiome is remarkably stable. a) Test phase drought treatment significantly reduced gamagrass shoot height (cm). Large points represent the estimated marginal mean (EMM) and the smaller points are the individual samples. b) Shannon diversity was not impacted by precipitation legacy or test phase water treatment. Points are EMMs and error bars represent the standard error. c) Test phase water treatment, but not legacy significantly impacted the gamagrass root microbiome composition. d) Drought treatment did not impact the root microbiome within group variation. Points are EMMs and error bars represent the standard error.

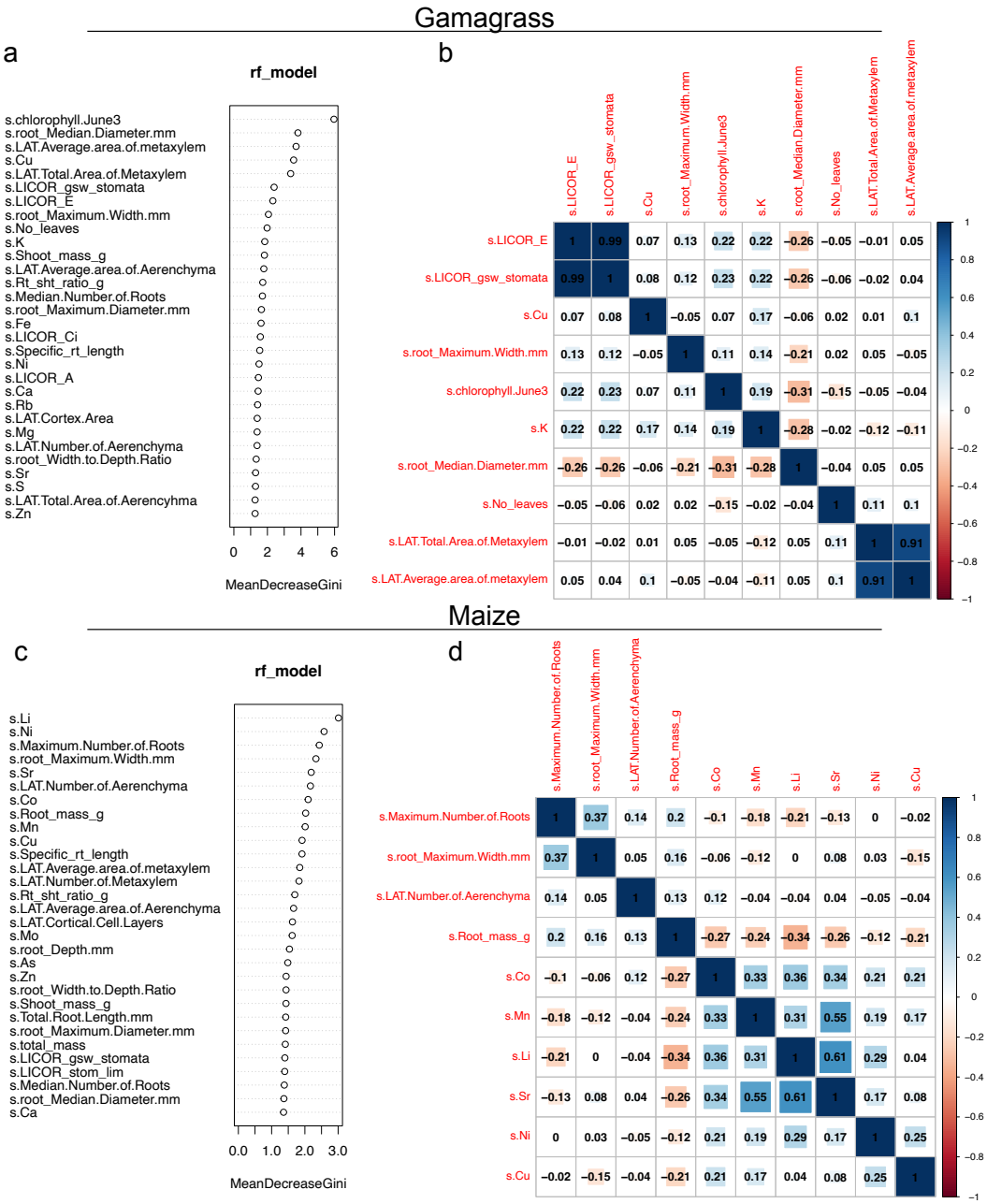

Extended Data Figure 7. Plant trait feature selection. Gamagrass (a-b) and maize (c-d) traits important in explaining legacy effects were ranked using a random forest model. The top ten traits were tested for significant correlations (≥0.7).

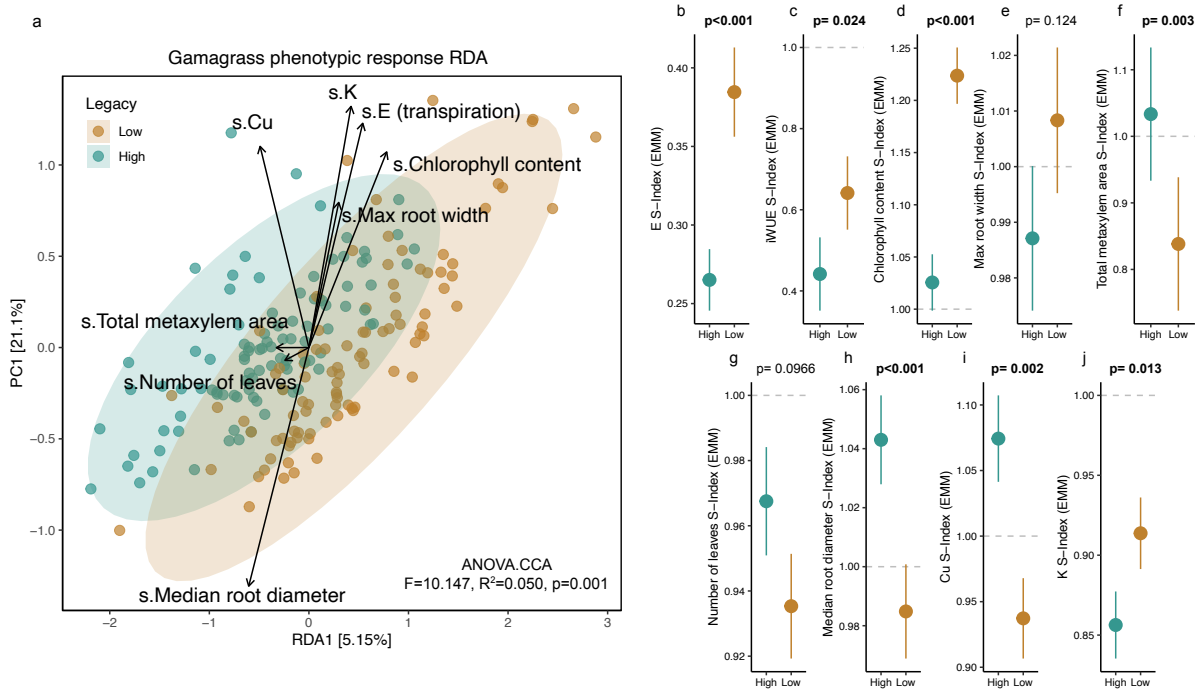

Extended Data Figure 8. Microbiome Legacy impacts gamagrass phenotypic drought response. a) A constrained redundancy analysis on the top non-correlated traits found that legacy explains 5.0% of gamagrass phenotypic response to acute drought. b-j) Assessment of individual traits indicates that microbiome drought legacy significantly improved gamagrass performance under drought. Points are EMMs and error bars represent the standard error, and significant p-values (≤0.05) are bolded.

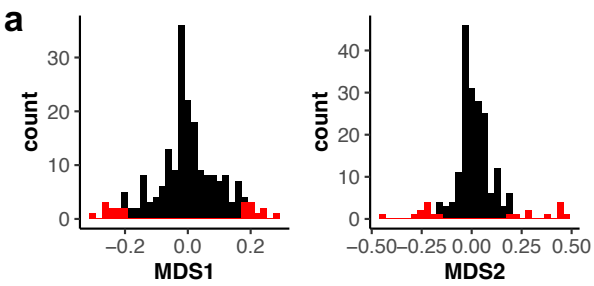

b

Number of genes		MDS1 +	MDS1 -
MDS2	+	52	54
	-	37	54

c

Top 5% of genes with strongest positive loadings on MDS1

Td_gene	MDS1	MDS2	Gene_set	Zm_orthologs	Zm_gene_symbol
Td00002ba000754	0.282	0.182	I	Zm00001eb057770	
Td00002ba018910	0.246	0.141	VII	Zm00001eb112460	cl31479_3
Td00002ba037703	0.241	-0.057	%	Zm00001eb237740	
Td00002ba002499	0.217	0.059	I	NA	
Td00002ba014047	0.21	0.021	I	Zm00001eb381580	
Td00002ba022717	0.208	0.065	III	Zm00001eb055100	
Td00002ba044330	0.205	0.103	VI	Zm00001eb199260	
Td00002ba019383	0.19	0.148	I	Zm00001eb115970	ms33
Td00002ba011993	0.181	0.078	I	Zm00001eb307550	ereb177
Td00002ba024147	0.178	0.057	I	Zm00001eb248540	umc2600a

Top 5% of genes with strongest positive loadings on MDS2

Td_gene	MDS1	MDS2	Gene_set	Zm_orthologs	Zm_gene_symbol
Td00002ba015526	-0.266	0.486	IV	Zm00001eb396120	nas7
Td00002ba015525	-0.259	0.46	IV	Zm00001eb396120	nas7
Td00002ba039891	-0.238	0.451	III	NA	
Td00002ba001144	0.168	0.447	VI	Zm00001eb053700	
Td00002ba001146	0.16	0.44	VI	Zm00001eb053700	
Td00002ba041411	-0.173	0.389	IV	NA	
Td00002ba015516	-0.141	0.272	IV	Zm00001eb396120	nas7
Td00002ba015515	-0.141	0.272	IV	Zm00001eb396120	nas7
Td00002ba033830	-0.15	0.218	V	Zm00001eb039280	ga20ox7
Td00002ba019393	-0.154	0.199	III	Zm00001eb286420	mads58

Top 5% of genes with strongest negative loadings on MDS1

Td_gene	MDS1	MDS2	Gene_set	Zm_orthologs	Zm_gene_symbol
Td00002ba046162	-0.203	0.116	V	Zm00001eb199320	
Td00002ba046161	-0.206	0.112	II	Zm00001eb199320	
Td00002ba036367	-0.222	0.138	II	Zm00001eb199320	
Td00002ba036368	-0.224	0.132	II	Zm00001eb199320	
Td00002ba019546	-0.236	-0.222	II	Zm00001eb147080	
Td00002ba039891	-0.238	0.451	III	NA	
Td00002ba007195	-0.257	0.113	II	Zm00001eb161990	
Td00002ba015525	-0.259	0.46	IV	Zm00001eb396120	nas7
Td00002ba015526	-0.266	0.486	IV	Zm00001eb396120	nas7
Td00002ba002239	-0.304	0.188	III	Zm00001eb048620	

% downregulated due to main effect of dry-legacy inoculum (no interaction with acute drought)

Top 5% of genes with strongest negative loadings on MDS2

Td_gene	MDS1	MDS2	Gene_set	Zm_orthologs	Zm_gene_symbol
Td00002ba023452	-0.061	-0.166	V	Zm00001eb027750	pat3
Td00002ba021901	0.012	-0.19	V	NA	
Td00002ba019546	-0.236	-0.222	II	Zm00001eb147080	
Td00002ba019177	0.023	-0.222	III	Zm00001eb180130	
Td00002ba009640	-0.077	-0.222	II	Zm00001eb210740	AY110625
Td00002ba008826	-0.138	-0.224	II	Zm00001eb125560	umc1742
Td00002ba045645	-0.019	-0.24	*	NA	
Td00002ba015343	0.124	-0.267	II	NA	
Td00002ba006731	-0.084	-0.272	II	Zm00001eb210740	AY110625
Td00002ba006546	-0.029	-0.435	VIII	Zm00001eb211300, Zm00001eb211310, Zm00001eb155430, Zm00001eb055690	pco095801, AY106518, GRMZM2G0249 58

* upregulated due to main effect of dry-legacy inoculum (no interaction with acute drought)

Extended Data Figure 9. Contributions of legacy-sensitive *Tripsacum dactyloides* genes to NMDS axes that mediate drought responses. (a) Histograms showing the distributions of gene loadings onto both axes. The top 5% of genes with the strongest positive and negative loadings onto each axis are in red. (b) Breakdown of the number of genes with positive/negative loadings onto each axis. (c) Lists of genes comprising the 5% tails of the distributions in (a). Detailed information about the expression responses of these genes is available in Supplementary Data 1. 'Gene_set' corresponds to the patterns of response to microbiome legacy presented in Figure 4a-b.

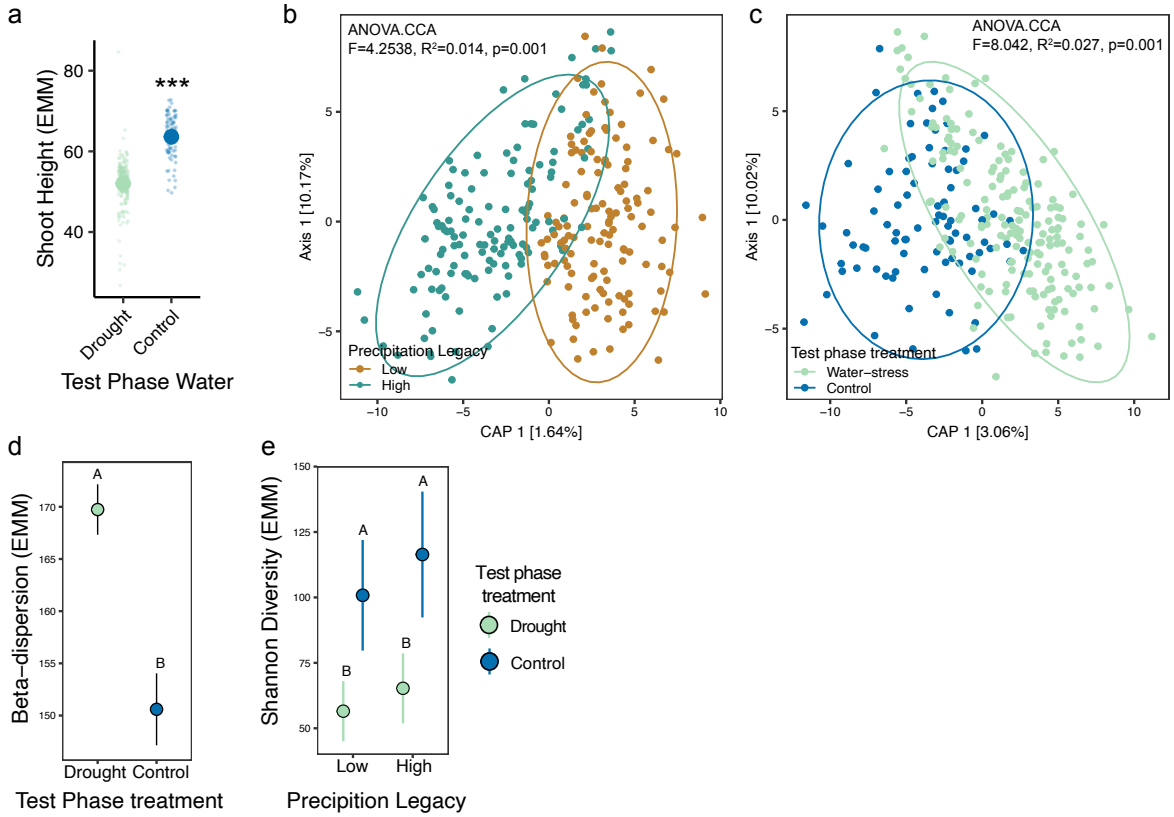

Extended Data Figure 10. Test phase maize root microbiome is impacted by legacy and acute drought treatment. a) Test phase drought treatment significantly reduced maize shoot height (cm). Large points represent the estimated marginal mean (EMM) and the smaller points are the individual samples. Legacy (b) and Test phase water treatment (c) significantly impacted the maize root microbiome composition. d) Acute drought treatment also increased maize root microbiome within group variation. Points are EMMs and error bars represent the standard error. Lastly, e) Shannon diversity was significantly impacted by test phase water treatment, but not legacy. Points are EMMs and error bars represent the standard error.

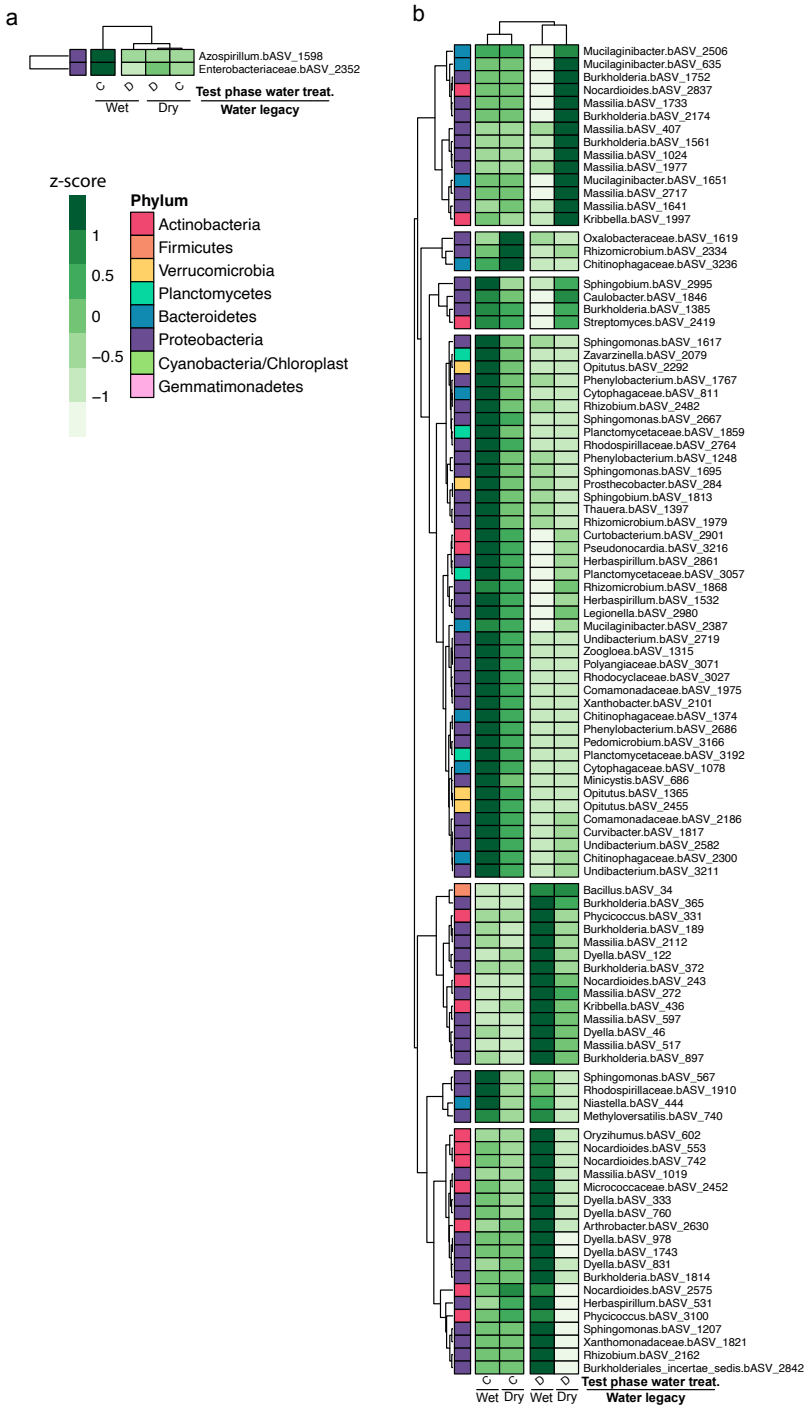

Extended Data Figure 11. Test phase water and legacy have a large impact on maize, but not gamagrass ASV abundance. Gamagrass root bacterial (a) and maize root bacterial (b) center-log ratio transformed ASV counts were individually fit to a linear to identify ASVs that were differentially abundant across test phase water treatments in the context of precipitation legacy. Dark green represents AVS enrichment and light green to white represents depletion. Multi-colored squares indicate phyla-level taxonomic assignments, which do not have an obvious phylogenetic pattern.

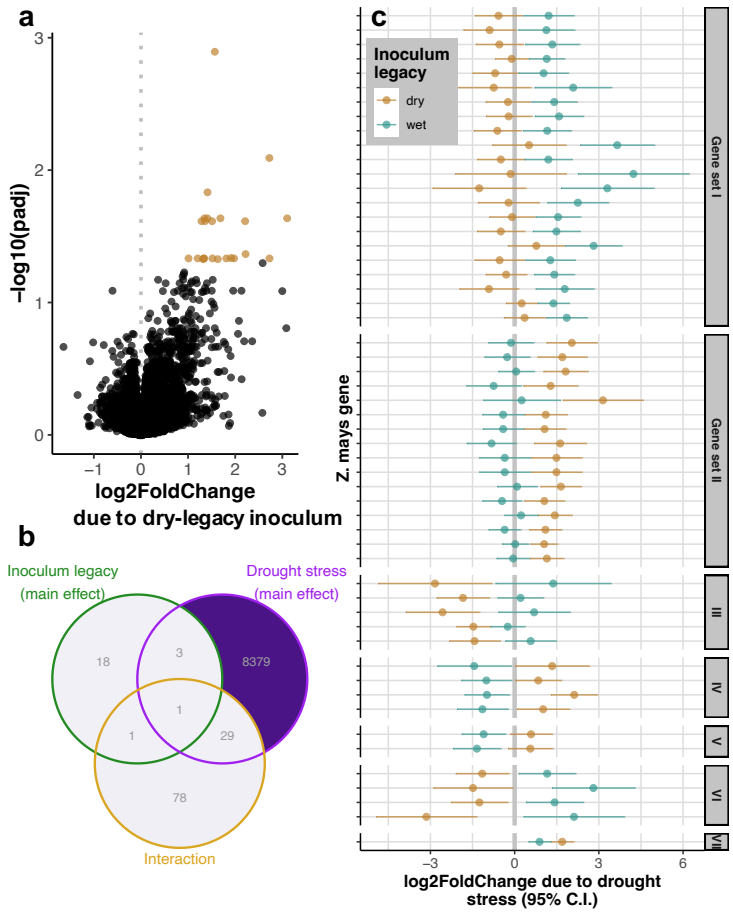

Extended Data Figure 12. Drought legacy of microbial inocula alters the transcriptional response to drought in the maize crown root. (a) 23 genes were up-regulated in plants inoculated with microbiota from a low-precipitation region, relative to plants inoculated with microbiota from a high-precipitation region. (b) The sets of genes that responded to the main effects of inoculum legacy and Test Phase drought stress had minimal overlap with each other or with the set of genes that were sensitive to the interaction between the two. (c) In total, 109 maize genes responded to drought in a manner that was dependent on the drought legacy of the soil microbiota, regardless of the inoculum's treatment during the conditioning phase. For illustration purposes, only annotated genes with a log2FoldChange> 1 in at least one microbial context are shown here; the full list is available in Supplementary Data 1. Each pair of points shows one gene; the relative position of the two points illustrates how the gene's expression changed in response to drought stress during the Test Phase, depending on whether the plant had been inoculated with microbiota derived from a low-precipitation or dry-precipitation environment. Genes are grouped into sets according to the pattern of how inoculum legacy altered their drought responses. Note: the names of these gene sets are not meant to correspond to the names of the *T. dactyloides* gene sets shown in Figure 4b; in each species, Gene set I contains the most genes, Gene set II contains the next most, and so on.

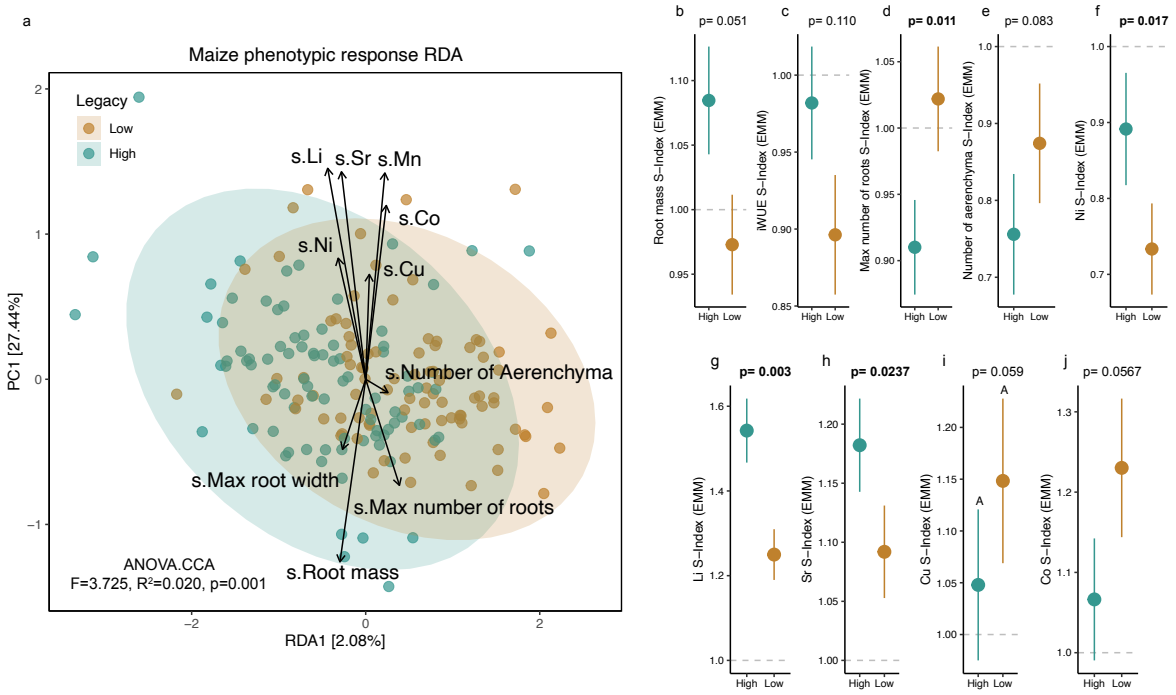

Extended Data Figure 13. Microbiome Legacy had minimal impact on maize phenotypic drought response. a) A constrained redundancy analysis on the top non-correlated traits found that legacy only explains 2.0% of maize phenotypic response to acute drought. b-j) Assessment of individual traits indicates that microbiome drought legacy did not significantly improve maize performance under drought, but did impact several mineral nutrient concentrations. Points are EMMs and error bars represent the standard error, and significant p-values (≤0.05) are bolded.